Supplementary Information

The Impact of Paleoclimatic Changes on Body Size Evolution in Marine Fishes

Emily M. Troyer[1,2], Ricardo Betancur-R[1], Lily C. Hughes[3], Mark Westneat[3], Giorgio Carnevale[4], William T. White[5], John J. Pogonoski[5], James C. Tyler[6], Carole C. Baldwin[7], Guillermo Ortí[8], Andrew Brinkworth[9], Julien Clavel[10], Dahiana Arcila[1,2*]

[1] Department of Biology, University of Oklahoma, 730 Van Vleet Oval, Richards Hall Norman, OK 73019, USA.
[2] Department of Ichthyology, Sam Noble Oklahoma Museum of Natural History, 2401 Chautauqua Avenue, Norman, OK 73072, USA.
[3] University of Chicago, Department of Organismal Biology and Anatomy, and Committee on Evolutionary Biology, 1027 E. 57th St, Chicago IL, 60637, USA.
[4] Università degli Studi di Torino, Dipartimento di Scienze della Terra, Torino, Italy.
[5] CSIRO Australian National Fish Collection, National Research Collections Australia, Castray Esplande, Hobart, Tasmania, Australia.
[6] Department of Paleobiology, National Museum of Natural History, Smithsonian Institution, 10th & Constitution Ave. NW, Washington, DC 20560, USA.
[7] Department of Vertebrate Zoology, National Museum of Natural History, Smithsonian Institution, 10th & Constitution Ave. NW, Washington, DC 20560, USA.
[8] The George Washington University, Department of Biological Sciences, Washington, D.C. 20052, USA.
[9] Milner Centre for Evolution, Department of Biology and Biochemistry, University of Bath, Bath, BA2 7AZ, UK.
[10] Univ Lyon, Université Claude Bernard Lyon 1, CNRS, ENTPE, UMR 5023 LEHNA, F-69622, Villeurbanne, France.

*Corresponding author: Dahiana Arcila
Email: dahiana.arcila@ou.edu

This PDF file includes:

Supplementary Materials and Methods
Figures S1 to S22
Tables S1 to S14
SI References

Other supplementary materials for this manuscript include the following:

Raw sequence reads for >1100 exon markers for all newly generated taxa (145 individuals representing 135 species) in this analysis. Uploaded to NCBI Sequence Read Archive under BioProject number PRJNA767646:

Dataset S1

A compressed folder containing all data files is available from Dryad (https://doi.org/10.5061/dryad.z34tmpgfw).

These include:

Datasets S2-S13

Supplementary Materials and Methods:

Taxonomic sampling and genomic data. We generated new genomic data from tissue samples extracted from museum voucher specimens (Dataset S1, Table S13) for 131 species of the order Tetraodontiformes and four species in its living sister clade, Lophiiformes (1). We shipped DNA extractions to Arbor Biosciences for library preparation and target enrichment. Libraries for all samples were processed at the sequencing facilities at the University of Chicago (https://fgf.uchicago.edu). Sequencing of pair end 100 bp reads was completed on a HiSeq 4000 with a total of 192 samples multiplexed per lane, including samples for other projects not listed here. Raw reads for newly sequenced exon-capture data are archived on NCBI Sequence Read Archive under BioProject number PRJNA767646 (Dataset S1). Target capture probes were based on a set of 1,105 single-copy nuclear exon markers (2, 3). Several of these 1,105 loci include "legacy" markers, which are popular markers within fish phylogenetics (4). One of the 131 newly sequenced species (*Rhinecanthus verrucosus*) was excluded due to low capture efficiency, leaving 130 newly sequenced taxa for use in downstream analyses. To increase taxonomic sampling, exon markers from four additional tetraodontiform species were mined from previously published genomes and transcriptomes (2) (Dataset S2). In addition, a total of 51 tetraodontiform species and one outgroup (Perciformes: *Antigonia capros*) were downloaded from NCBI; these include sequences from one mitochondrial and 15 nuclear markers (1, 3–5) (Dataset S2). The final molecular matrix includes a total of 185 out of *ca.* 450 extant tetraodontiforms (~41.1%) representing all 10 extant families.

Alignment and quality control. Sequences for each exon were aligned with MACSE v 2.03 (6) after cleaning out potentially non-homologous fragments with the -cleanNonHomologousSequences option. Separate alignments were conducted, including the target exon in MAFFT v. 7.427 (7). All alignments were visually inspected to adjust the reading frames, remove poor-quality reads, and correct misaligned sections in Geneious Prime v. 2020.1.1 (8). Alignment summary statistics, such as the percentage of missing data, GC content, proportion of variable sites, and alignment length was assessed using the python package AMAS (9) (Dataset S8).

Given the pervasiveness of contamination in phylogenomic datasets, quality control analyses consisted of visual inspection of individual gene trees estimated in IQTREE v.1.6.12 (10) and manual inspection of individual gene alignments, following the pipeline implemented by Arcila et al. (11). Additional steps of quality control included cross-validating species identifications of all newly sequenced tissue samples by blasting the mtDNA-COI barcode region against the Barcode of Life Data System (BOLD) repositories (12) using the 'bold_identification' python script (13) (Dataset S10). After these quality control steps, two of the newly sequenced exons were deleted from the analysis due to high levels of missing data, leaving a total of 1,103 loci.

Phylogenomic inference. We inferred phylogenetic trees and support values using maximum likelihood with IQTREE v.1.6.12 (10) and a multi-species coalescent approach in ASTRAL-III (14) based on IQTREE gene trees. To account for the effects of missing data in our dataset, we conducted two concatenation-based maximum likelihood (ML) analyses: one including all newly sequenced taxa (134 tetraodontiform species, 47% missing data overall; Dataset S6), and a second analysis that excluded taxa with more than 65% missing data (102 tetraodontiform

species, < 33% missing data overall; Dataset S7) for all 1,103 exon markers. Because the topology and branch lengths are largely in agreement between the two analyses (*SI Appendix:* Figs. S2, S3), all downstream phylogenetic analyses use the complete dataset (134 tetraodontiform species and 1,103 exon markers). We used PartitionFinder2 (15) to infer the best partitioning scheme for the concatenated datasets, beginning with a total of 3,309 *a priori* partitions (three codon positions for each of the 1,103 loci). From these initial partitions, a best-fit scheme of 719 partitions was identified and used as input for all ML phylogenetic analyses. Each of the 719 partitions used a substitution model of either GTR+G or GTR+I+G.

To account for discordance arising from incomplete lineage sorting (ILS), we conducted a multi-species coalescent analysis with multi-locus bootstrapping in ASTRAL-III (14) (Dataset S5) using 1,103 unrooted individual gene trees (partitioned by codon position) inferred from IQTREE (Dataset S4). We estimated branch support for all gene trees in IQTREE using the ultra-fast bootstrapping approach with 1,000 replicates implemented using the '-bnni' option (16). We used bootstrap replicates for each gene as input for ASTRAL, as well as all 1,103 maximum likelihood gene trees.

Integration of fossil and extant species. To combine the fossils and extant tetraodontiform species, we used the morphological matrix of Arcila and Tyler (17), which consists of 210 characters coded for 17 extant and 52 fossil tetraodontiform species plus two additional outgroup taxa (Lophiiformes: *Lophiodes monodi*, and Zeiformes: *Cyttus novaezelandiae*). We combined this morphological matrix with our genomic dataset for a total of 237 tetraodontiform species and seven outgroups. Our analyses use the GTRGAMMA and Mk models with four partitions; three for the molecular sequences (one for each codon position); and one for the morphological dataset.

Phylogenetic uncertainty and total evidence dating using the fossilized birth death process. In addition to the phylogenomic analyses described above, we conducted divergence time estimations under a total evidence, or tip-dating, framework using the Fossilized Birth Death (FBD) model in MrBayes v 3.2.7a (18). To account for topological uncertainty, we assembled 15 largely independent genomic subsets containing *ca.* 50 randomly selected loci (~20,000 bp) subsampled from the complete genomic dataset of 1,103 loci. All subsets overlap in only five "anchor" genes to maintain the same set of species for each subset (19, 20). In addition to genomic data, each subset contains the morphological dataset for fossil taxa. We ran all 15 subsets in MrBayes with tree sampling occurring every 10,000 generations. We used a relaxed clock model with the clock rate prior following a log normal distribution and independent gamma rate (IGR). After 6 months of total runtime, we found that only 5 (of the 15) subsets reached convergence based on estimated sample size (ESS) values close to or above 200. After filtering out analyses that fail to converge, we updated the root prior ages with different distributions and added certain phylogenetic constraints, described below.

Updated subset schemes (root priors and the inclusion/exclusion of Plectocretacicoidea). Because there is not yet consensus on whether the superfamily Plectocretacicoidea should be considered as stem tetraodontiforms and the exclusion of this superfamily has the potential to drastically affect age estimations (17, 21), we used two different schemes including and excluding the plectocretacicoids for a total of 10 subsets. This superfamily, containing four extinct taxa, are some of the oldest acanthomorph fish fossils and share 14 morphological

synapomorphies with Tetraodontiformes (17). The first scheme includes plectocretacicoids in the analysis and places the oldest fossil calibration age at 95 Ma, the minimum age of the oldest plectocretacicoid fossil (*Plectocretacicus clarae*†). The second analysis excludes plectocretacicoids and the oldest fossil calibration is 59 Ma, based on the minimum age of the oldest fossil (*Moclaybalistes danekrus*†) assigned to crown tetraodontiforms.

To test if the tree age prior influences the root age, we assigned three of the five subsets in each scheme a uniform distribution and the remaining two an offset exponential distribution for the tree age prior. For the subset scheme inclusive of Plectocretacicoidea, the uniform distribution has a minimum age of 95.9 Ma and maximum age of 110, and the offset exponential distribution has a minimum age of 95 Ma and mean age of 107.9. In the subset scheme exclusive of Plectocretacicoidea, the uniform distribution has a minimum age of 59 Ma and maximum age of 67.43 Ma, and the offset exponential distribution has a minimum age of 59 Ma and mean age of 61.8 Ma. To examine potential effects of the root prior distribution on the posterior estimations, we ran each distribution scheme (uniform distribution and offset exponential) without data for both fossil schemes (with and without Plectocretacicoidea; Tables S1-S4).

We placed constraints onto extant tetraodontiform families, as their monophyly is not debated, but rather how they are placed at the short inner branches at the base of the tree. In addition, we placed constraints for: Tetraodontoidea (Diodontidae+Tetraodontidae), Balistoidea (Balistidae+Monacanthidae), Triacanthoidea (Triacanthidae+Triacanthodidae), Ostracioidea (Ostraciidae+Aracanidae), and Plectocretacicoidea†. We also included constraints on fossil families and fossil genera for Bolcabalistidae†, Monacanthidae+ Bolcabalistidae†, *Zignoichthys*†+*Iraniplectus*†+Molidae, Triodontidae+Ctenoplectus†, Ostracioidea+*Protobalistum*†+*Spinacanthus*†, Tetraodontoidea+*Balkaria*†. Lastly, we assigned additional constraints for all Tetraodontiformes, all Lophiiformes, all Percomorpha, and a root constraint.

We ran the updated subset schemes in MrBayes until convergence (around 100-150 million generations, depending on the exact subset) and we combined all runs for each subset after discarding 10% of the first tree sampled as burn-in. We evenly sampled 100 trees (i.e. we took every nth tree until 100 trees were obtained) from the posterior distribution of each subset in a given scheme to take into account phylogenetic uncertainty for downstream comparative analyses, for a total of 500 trees. In addition, we constructed a maximum clade credibility (MCC) tree from 10,000 trees evenly sampled from the posterior of all five subsets using TreeAnnotator (22) (Dataset S11, S12).

Trait data. We compiled total length (TL) and standard length (SL) data for most fossil and extant tetraodontiform species in our dataset, targeting five individuals per species when possible (Dataset S3). We obtained length data for extinct species from museum collection databases (e.g., Smithsonian National Museum of Natural History) and published papers, and data for extant species from published papers, museum collections, and FishBase (23). In the case where TL was the only measurement reported in a dataset, we estimated the equation for SL, for each tetraodontiform family, based on species measurements where both TL and SL were known (Dataset S13). Because of the bias for smaller specimens in museum collections, we omitted any measurements from individuals that were more than 20% smaller than the maximum recorded size listed on FishBase, leaving one to three individuals per species which were averaged to obtain a mean maximum SL per species. We chose maximum SL values as an indicator for how large a species could potentially reach. We excluded three of the extinct tetraodontiform species

(*Archaeotetraodon cerrinaferoni*†, *Archaeotetraodon dicarloi*†, and *Ctenoplectus williamsi*†) from the body length analyses due to incomplete or fragmented fossils, which precluded SL from being accurately assessed. We performed all analyses using log transformed values.

Because many species of tetraodontiform fishes are irregularly shaped (i.e. boxfishes, pufferfishes, etc.), we assessed the robustness of using SL as a proxy for body size compared to other measurements such as volume and surface area (SA) in a subset of tetraodontiform species, representing all 10 extant families. Using publicly available computed-tomography (CT) scan data accessed from MorphoSource.org for 27 species of tetraodontiforms in addition to newly collected CT scan data for 14 species (Dataset S9), we created three-dimensional models using the image computing platform Slicer(24). To accurately calculate volume and surface area, we solidified models using the WrapSolidify option in the Segment Editor module and calculated volume (mm^3) and SA (mm^2) using the Segment Statistics module. We measured the SL of the models using the ruler tool. We log-transformed all measurements and performed phylogenetic generalized least squares (PGLS) analyses between SL and volume, and SL and SA. PGLS between SL and volume revealed a strong positive correlation ($p = 0.0005$; *SI Appendix*, Fig. S13). A similar pattern was found for SL and SA ($p = 0.0248$; *SI Appendix*, Fig. S14). Because the resulting measurements were highly correlated to SL across the majority of extant tetraodontiform families, we opted to simply use SL as a proxy for body size. In addition to the simplicity of calculating SL for each extant species in our dataset, SL is easily obtained from fossil taxa, whereas other measurements, such as volume or SA, are impractical to obtain for such species.

Paleotemperature data. We obtained temperature curves that span the nearly 100 Ma evolutionary history of tetraodontiforms from Scotese et al. (25). These authors used oxygen isotope data to reconstruct past global average ocean temperatures and sea surface temperatures between tropical latitudes (15°N-15°S). Given the broad distributions (circumtropical/subtropical latitudes) and habitat preferences (mainly marine shallow-water, but also deep-water, estuarine, and freshwater dwellers) of tetraodontiforms, these two contrasting temperature curves most accurately capture the spectrum of past environmental affinities in this group.

Evolutionary model fitting. We conducted model fitting analyses in R version 4.0.2 (26). We fitted models of continuous character evolution using the R package 'geiger' and the 'fitContinuous' function. We selected two standard models of evolution: a Brownian motion (BM) model, where body size is expected to be randomly dispersed through time and an Ornstein-Uhlenbeck (OU) model, which is similar to a BM model, but with a tendency for a trait to move towards a central optimum. In addition, we fitted evolutionary rate models which include an early burst (EB) model where the rate of trait evolution is initially high, then decreases exponentially over time and a rate trend model which fits a linear trend in evolutionary rates through time (either towards a larger or smaller rate of evolution). To test Cope's rule, we fitted a mean trend (or drift) model, which fits a directional trend component (i.e. towards a larger or smaller body size through time). To more explicitly assess an increase in body size in response to paleoclimatic changes over time (Cope-Bergmann rule), we fitted a climate-dependent OU model (Eq. 1), which is an extension of the classical OU process and has a time-dependent optimum $\theta(t)$ (27).

$$dX(t) = \alpha[\theta(t) - X(t)]dt + \sigma dB(t) \qquad (1)$$

We tested this model using the two temperature curves mentioned above from Scotese et al. (25). We considered the best fitting model to be that with the lowest corrected Akaike information criteria (AICc) score. To account for tree uncertainty, we tested all models with the 500 trees selected from the posterior distribution. Additionally, we account for interspecific variation by incorporating measurement error into our comparative analyses by calculating the standard error of the mean for each species (standard deviation of SL/number of individuals) and incorporating this into the model fitting analyses.

Because there is a global trend towards declining temperatures over the evolutionary history of Tetraodontiformes (i.e. from the late Cretaceous to present day), it can be difficult to decouple the effects of temperature (Bergmann's Rule) from other processes that may be correlated to increased body sizes (Cope's Rule). To disentangle the effects of the long-term cooling trend from the main cyclic fluctuations of temperatures over the past 100 Ma, we decomposed the temperature curves and constructed an alternate "decomposed" OU climate model which uses two additional parameters: the overall trend and the variations around this trend (Fig. S13). To assess which parameter was most important to model fit, we ran three analyses on both temperature curves (GAT and tropical latitudes). The first analysis modeled the two independent components (overall trend and variations) together, the second modeled only the overall trend, and the third modeled only the variations (Fig. S14).

Ecomorphological correlations. To further determine if tetraodontiforms adhere to the Cope-Bergmann rule, we examined patterns of body size in relation to past ocean temperature changes for the two temperature curves mentioned above. We performed ancestral state reconstructions of body sizes for all nodes and mapped these onto the MCC tree using the 'contMap' function in the R package 'phytools' (28). This function maps estimated states at internal nodes using maximum likelihood and the 'fastAnc' function under a Brownian motion model. To take phylogenetic independence into account, we performed a phylogenetic generalized least squares (PGLS) analysis on each temperature curve from Scotese et al. (25). Because a PGLS requires tips as input, we modify our MCC tree by grafting branches with zero lengths onto each node of the MCC tree. These we now consider "tips" which can be assigned the estimated ancestral body size reconstructions for use in the analyses. Using the 'gls' function in the R package 'nlme', we first compared a set of evolutionary models including PGLS under a Brownian Motion (PGLS-BM) model, an Ornstein-Uhlenbeck (PGLS-OU) model, and a model where phylogeny is not considered (i.e. Ordinary Least Squares or OLS). Because the 'gls' function requires an input tree, the OLS regressions were run after transforming species covariances by a Pagel's λ value of 0 using the 'lambdaTree' function in the 'phytools' package .

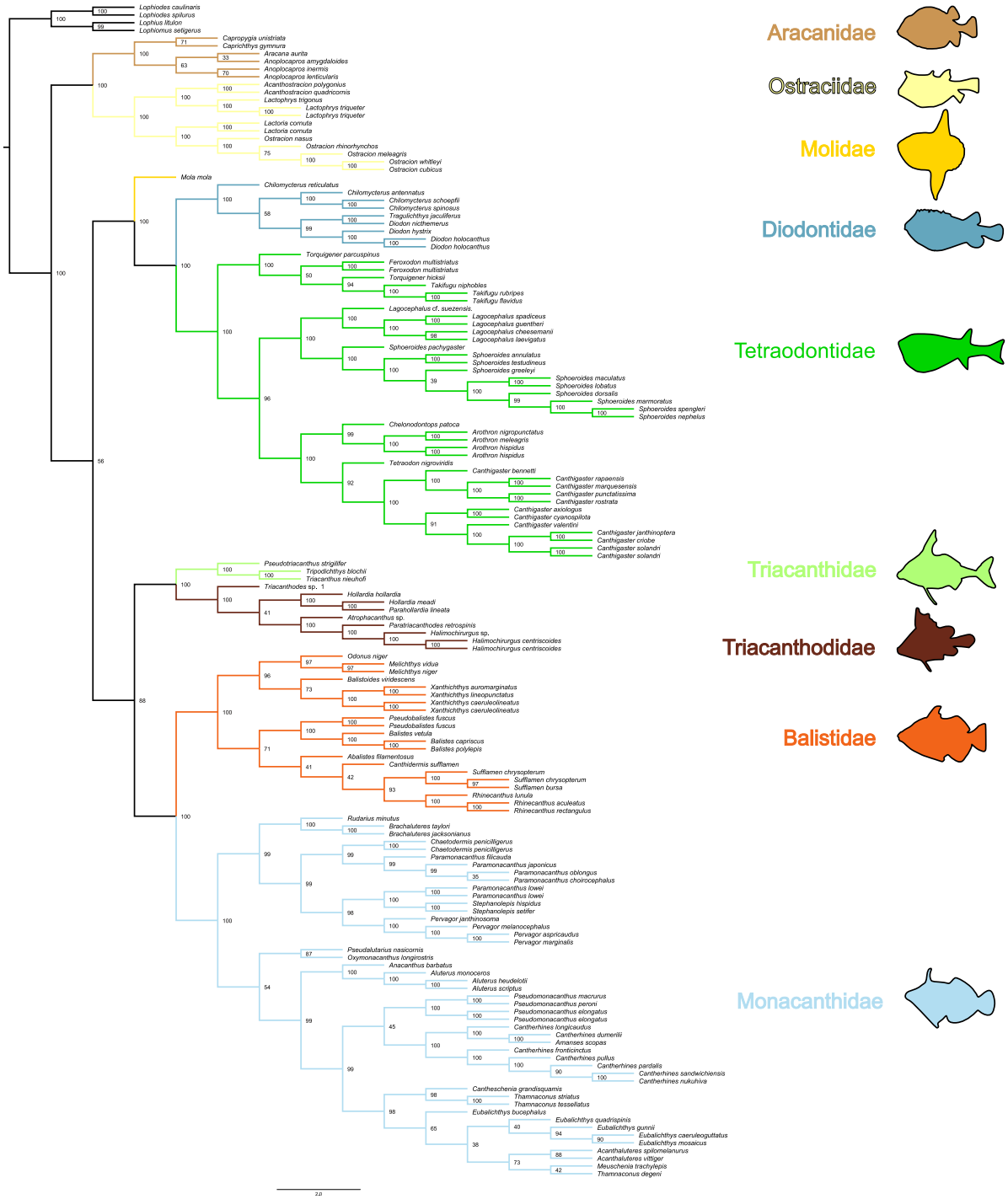

Fig. S1. Phylogeny of Tetraodontiformes based on multi-species coalescent analysis of 1,103 exons and 138 species (134 Tetraodontiformes, 4 outgroup Lophiiformes). Phylogenetic tree inferred with ASTRAL for all newly sequenced taxa and four previously published transcriptomes (3). Colors indicate families. Nodal values indication bootstrap support. Tree is a cladogram and branch lengths do not represent any evolutionary distance.

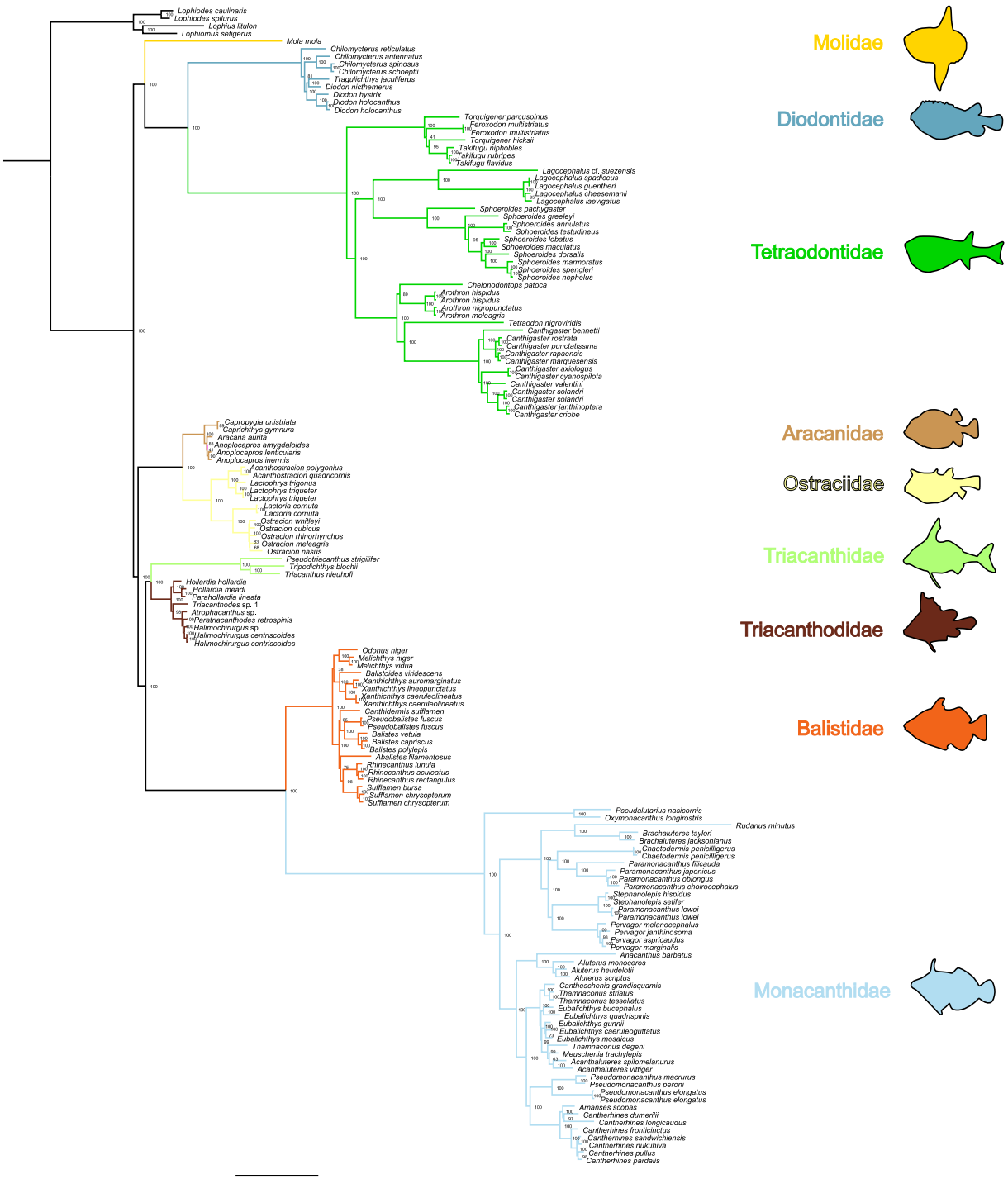

Fig. S2. Phylogeny of Tetraodontiformes based on concatenation analysis of 1,103 exons and 138 species (134 Tetraodontiformes, 4 outgroup Lophiiformes). Phylogenetic tree inferred with IQTREE using the best fit partition scheme identified with PartitionFinder for all newly sequenced taxa and four previously published transcriptomes (3). Colors indicate families. Nodal values indication bootstrap support. Branch lengths are the number of nucleotide substitutions per nucleotide site.

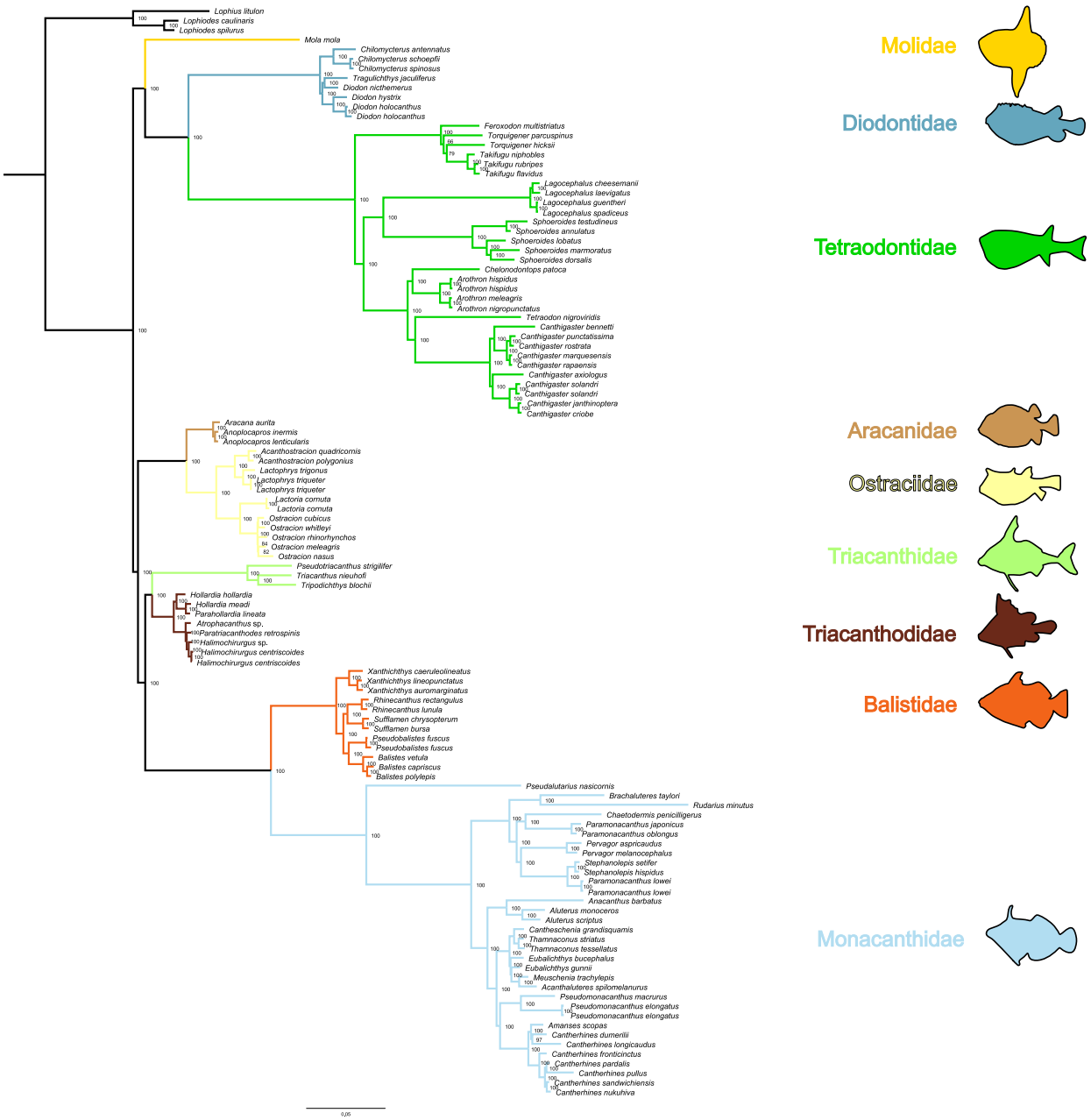

Fig. S3. Phylogeny of Tetraodontiformes, excluding taxa with more than 65% missing data, based on concatenation analysis of 1,103 exons and 105 species (102 Tetraodontiformes, 3 outgroup Lophiiformes). Phylogenetic tree inferred with IQTREE using the best fit partition scheme identified in PartitionFinder for all newly sequenced taxa and four previously published transcriptomes (3). Colors indicate families. Nodal values indication bootstrap support. Branch lengths are the number of nucleotide substitutions per nucleotide site.

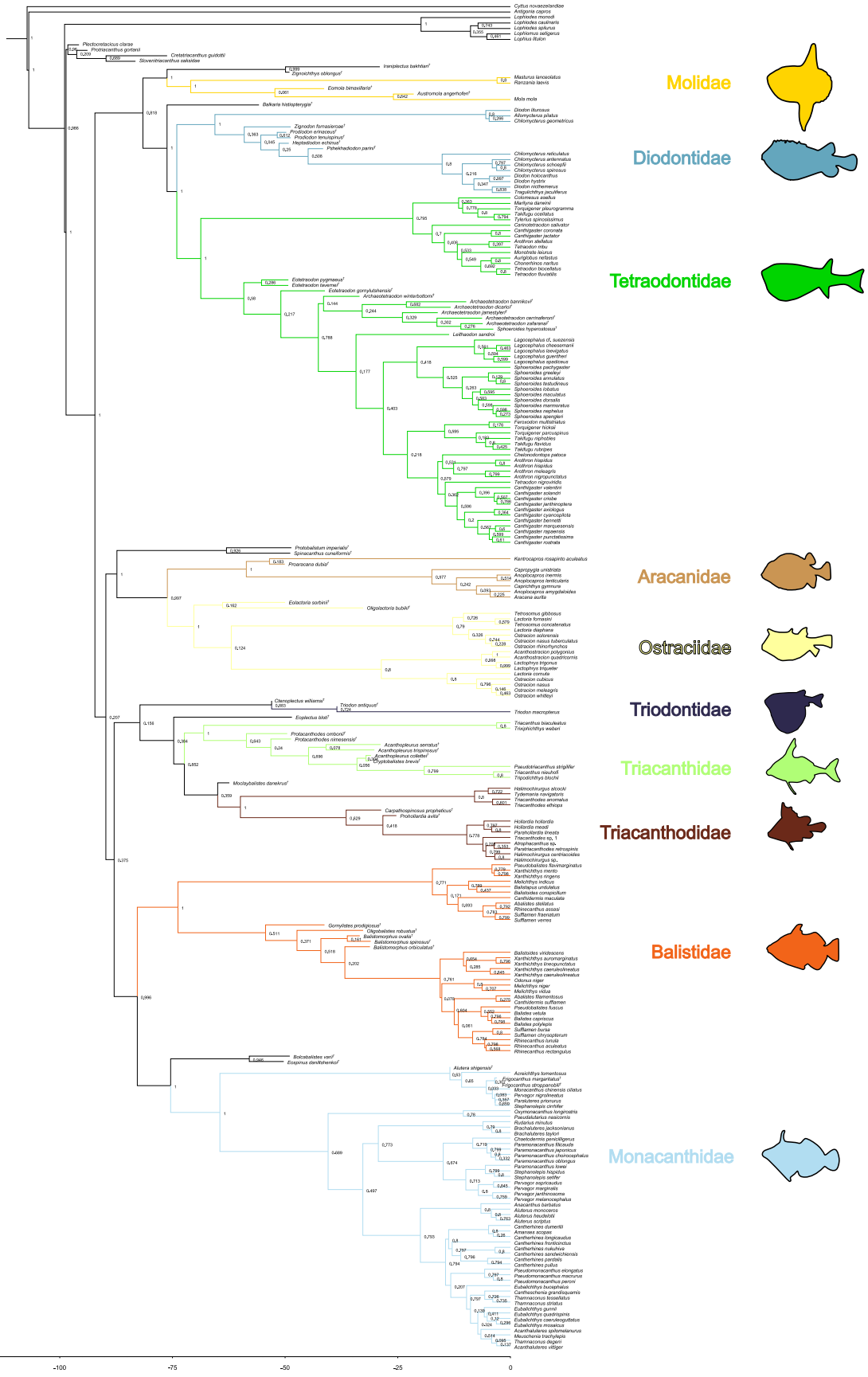
Molidae
Diodontidae
Tetraodontidae
Aracanidae
Ostraciidae
Triodontidae
Triacanthidae
Triacanthodidae
Balistidae
Monacanthidae
-125
-100
-75
-50
-25
0

Fig. S4. Maximum clade credibility (MCC) tree of Tetraodontiformes. Time-calibrated phylogenetic tree using a total-evidence framework based on Bayesian inference of 1,103 exons and 237 tetraodontiforms (52 fossil, 185 extant) and seven outgroups. MCC tree generated from 10,000 trees evenly selected from the posterior distribution of five subsets. Colors indicate families. Scale bar represents millions of years. Posterior probability values are given for each node.

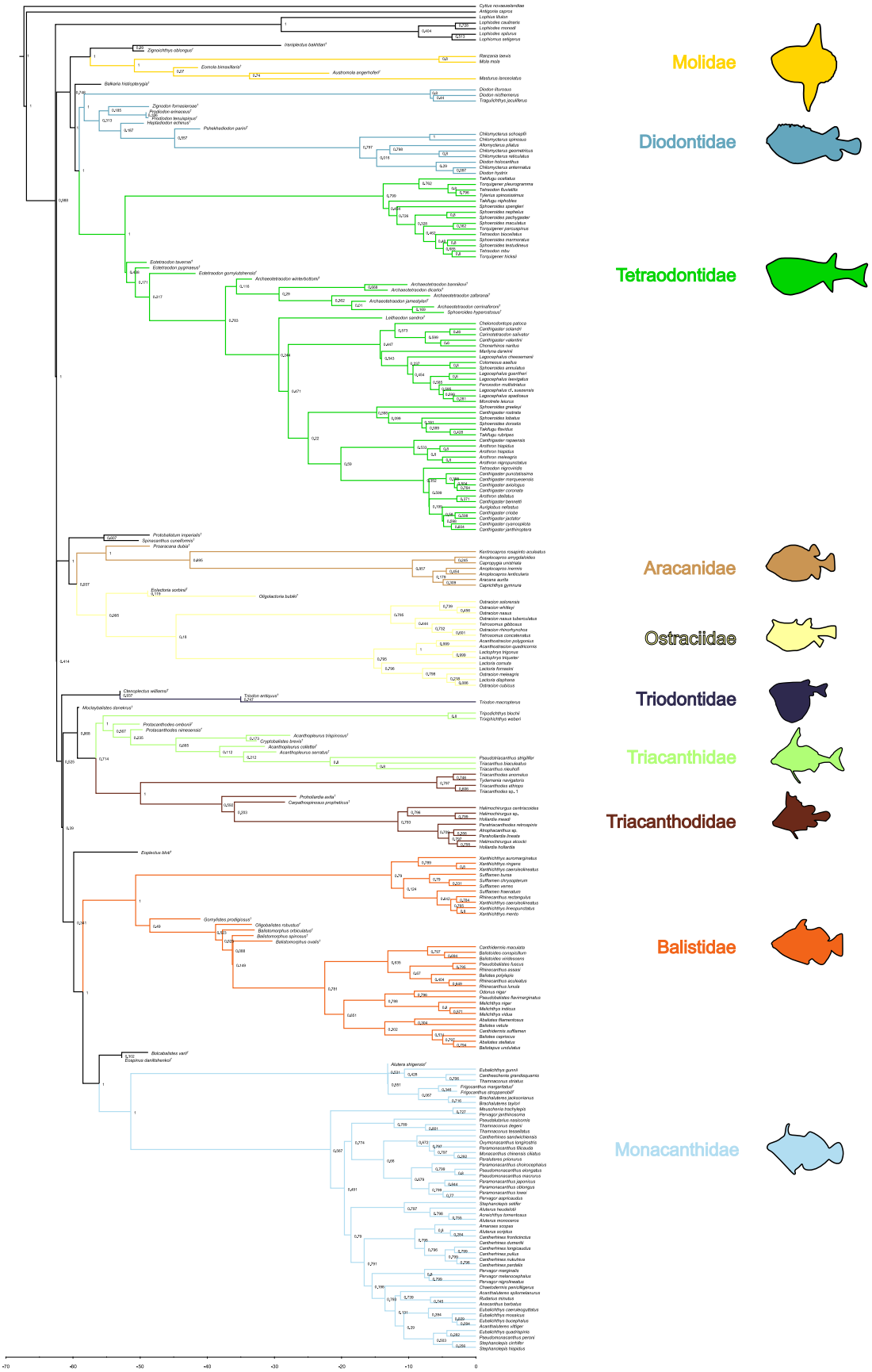
Molidae
Diodontidae
Tetraodontidae
Aracanidae
Ostracidae
Triodontidae
Triacanthidae
Triacanthodidae
Balistidae
Monacanthidae
-70
-60
-50
-40
-30
-20
-10
0

Fig. S5. Maximum clade credibility (MCC) tree of Tetraodontiformes, excluding the superfamily Plectocretacicoidea. Time-calibrated phylogenetic tree using a total-evidence framework based on Bayesian inference of 1,103 exons and 233 tetraodontiforms (48 fossil, 185 extant) and seven outgroups. MCC tree generated from 10,000 trees evenly selected from the posterior distribution of five subsets. Colors indicate families. Scale bar represents millions of years. Posterior probability values are given for each node.

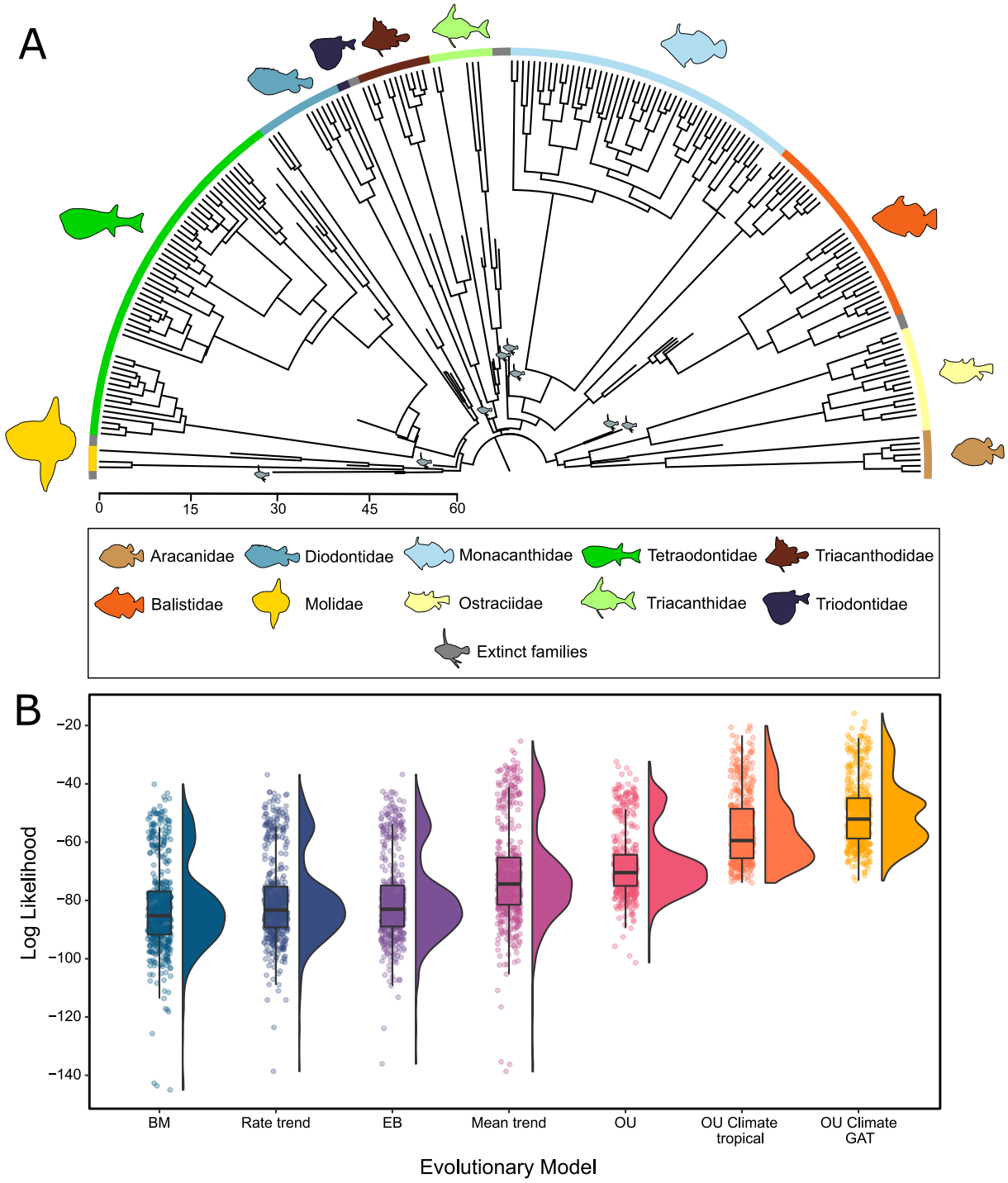

Fig. S6. Tip-dating tree inferred for tetraodontiforms and evolutionary model fitting results, excluding superfamily Plectocretacicoidea. *A*, Maximum clade credibility (MCC) tree derived from a total-evidence dating analysis using the fossilized birth-death model in MrBayes (excluding plectocretacicoids). MCC tree is derived from 10,000 trees evenly sampled from the posterior distribution of five independent subsets. See *SI Appendix*, Fig. S5 for an expanded version of this tree. ***B*,** Raincloud plots (half-violin plots and boxplots) for each model of body

size evolution tested, representing the distribution of likelihood scores from 500 trees evenly selected from the posterior distribution of five gene subsets in the Bayesian analysis (see also Table S6). Dots represent raw likelihood score for each of the 500 trees analyzed, for each model. Evolutionary models tested include Early-burst (EB), Brownian motion (BM), rate trend, Ornstein-Uhlenbeck (OU), mean trend, a climate OU model using tropical ocean temperatures, and a climate OU model using global average ocean temperatures (GAT).

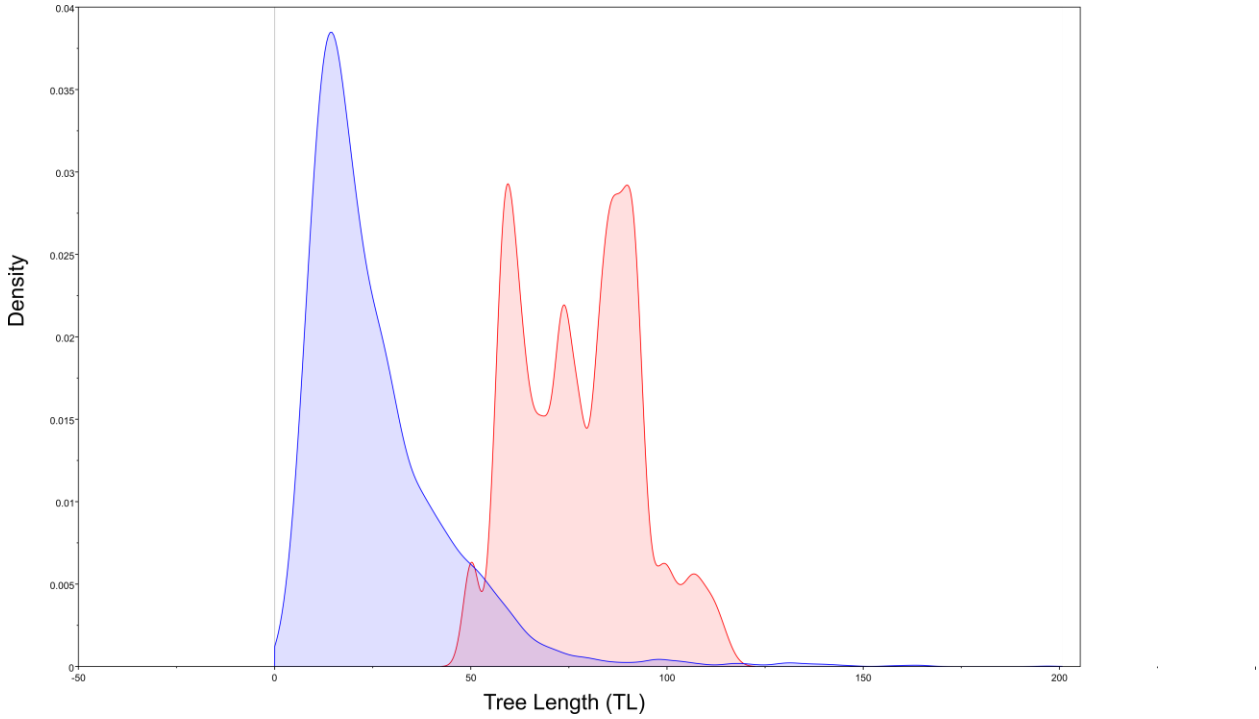

Fig S7. Kernel density plot for the tree length (TL) prior for a subset run with data (purple) and without data (green).

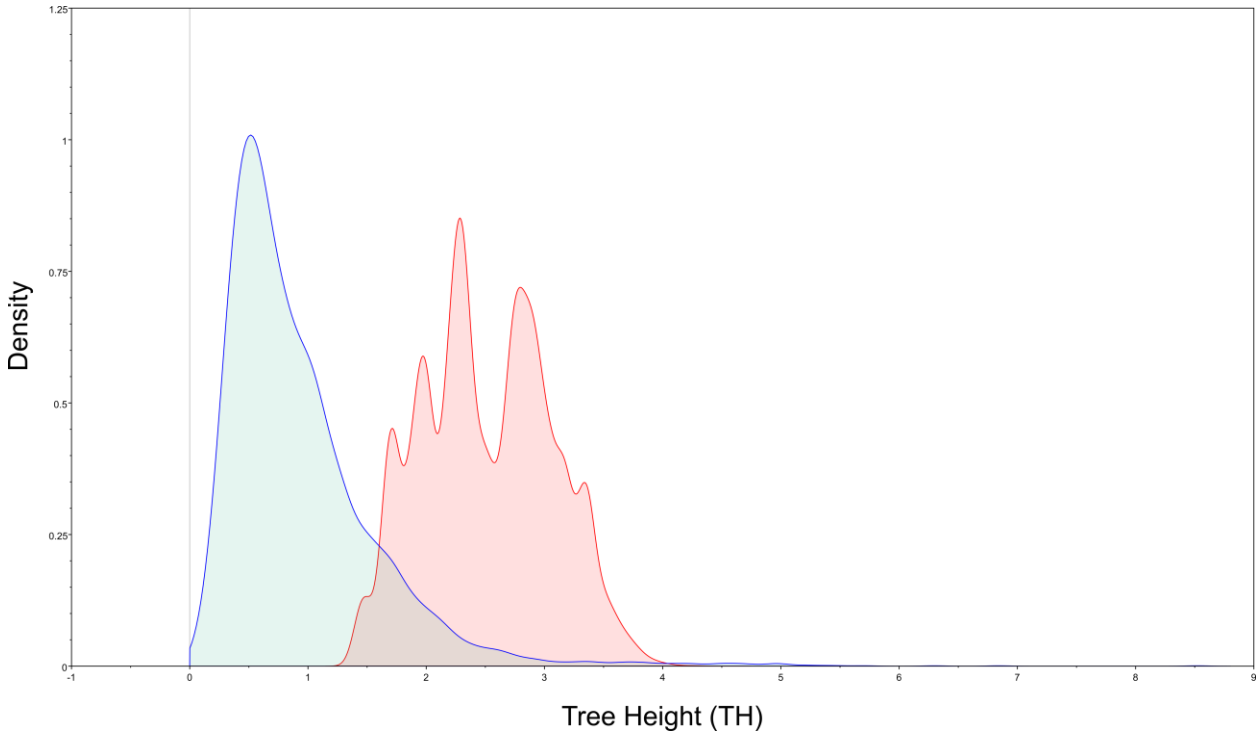

Fig. S8. Kernel density plot of the tree height (TH) prior for subset run with data (blue) and without data (red)

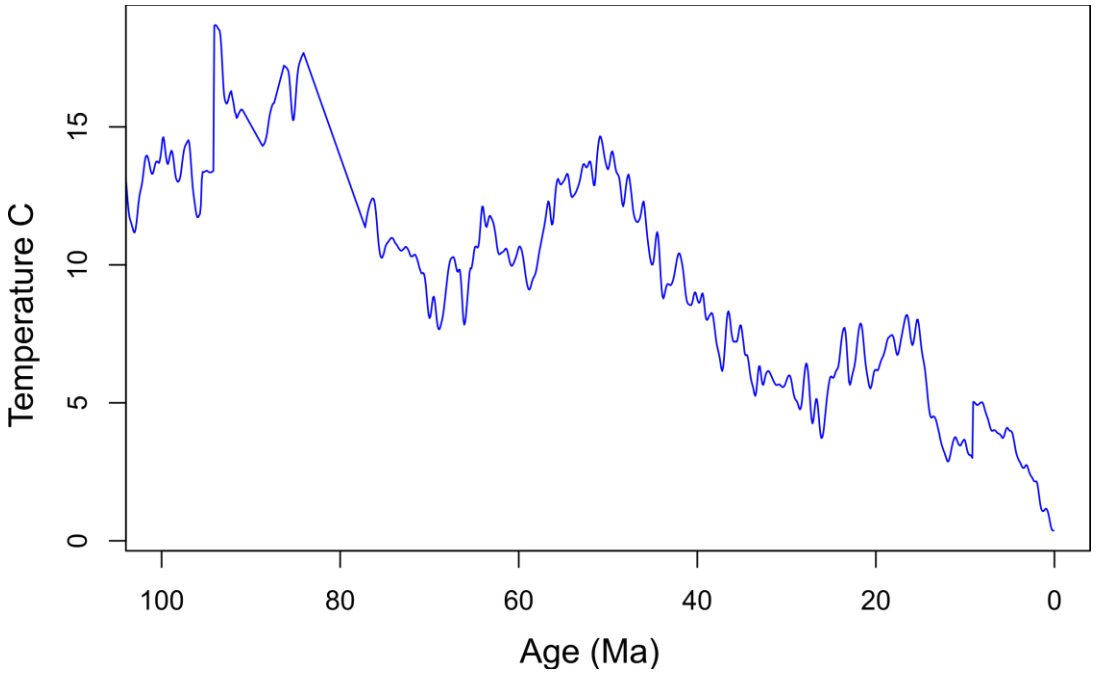

Fig. S9. Deep-sea temperature curve for the past 100 Ma based on data from Cramer et al. (33)

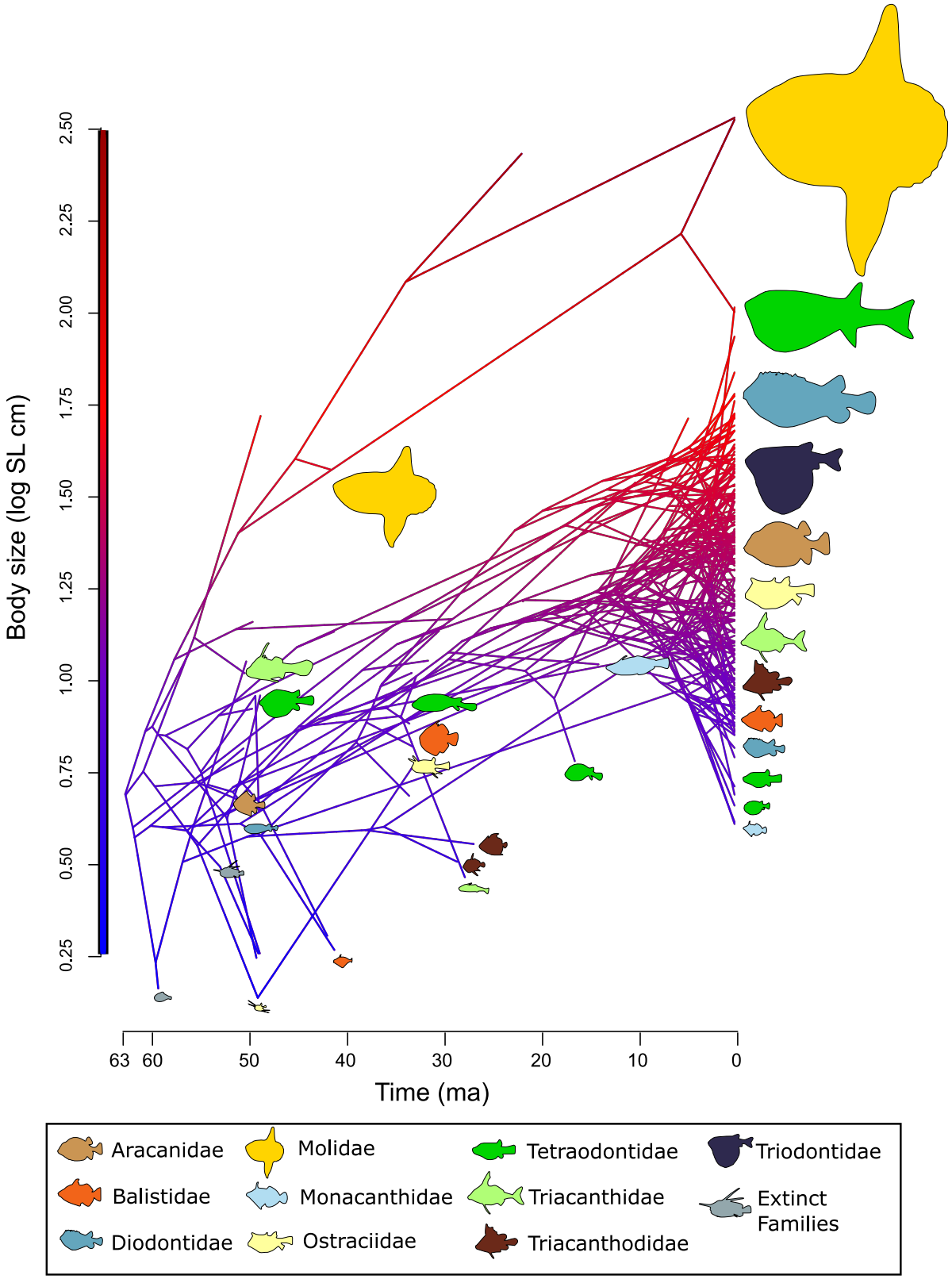
Body size (log SL cm)
0.25
0.50
0.75
1.00
1.25
1.50
1.75
2.00
2.25
2.50
63
60
50
40
30
20
10
0
Time (ma)
Aracanidae
Balistidae
Diodontidae
Molidae
Monacanthidae
Ostraciidae
Tetraodontidae
Triacanthidae
Triacanthodidae
Triodontidae
Extinct Families

Fig. S10. Evolution of tetraodontiform body size over time, excluding superfamily Plectocretacicoidea. Ancestral reconstruction of body size in tetraodontiforms, as estimated using the R package ‘phytools’ (28). The log-transformed mean maximum standard length for each species is plotted as a traitgram on the Y axis, with time on the X axis. Fish silhouettes are scaled to represent proportional log body size and colored by family, with extinct families in grey. The estimated ancestral body size of tetraodontiforms is 2-3 times smaller than that of present-day taxa.

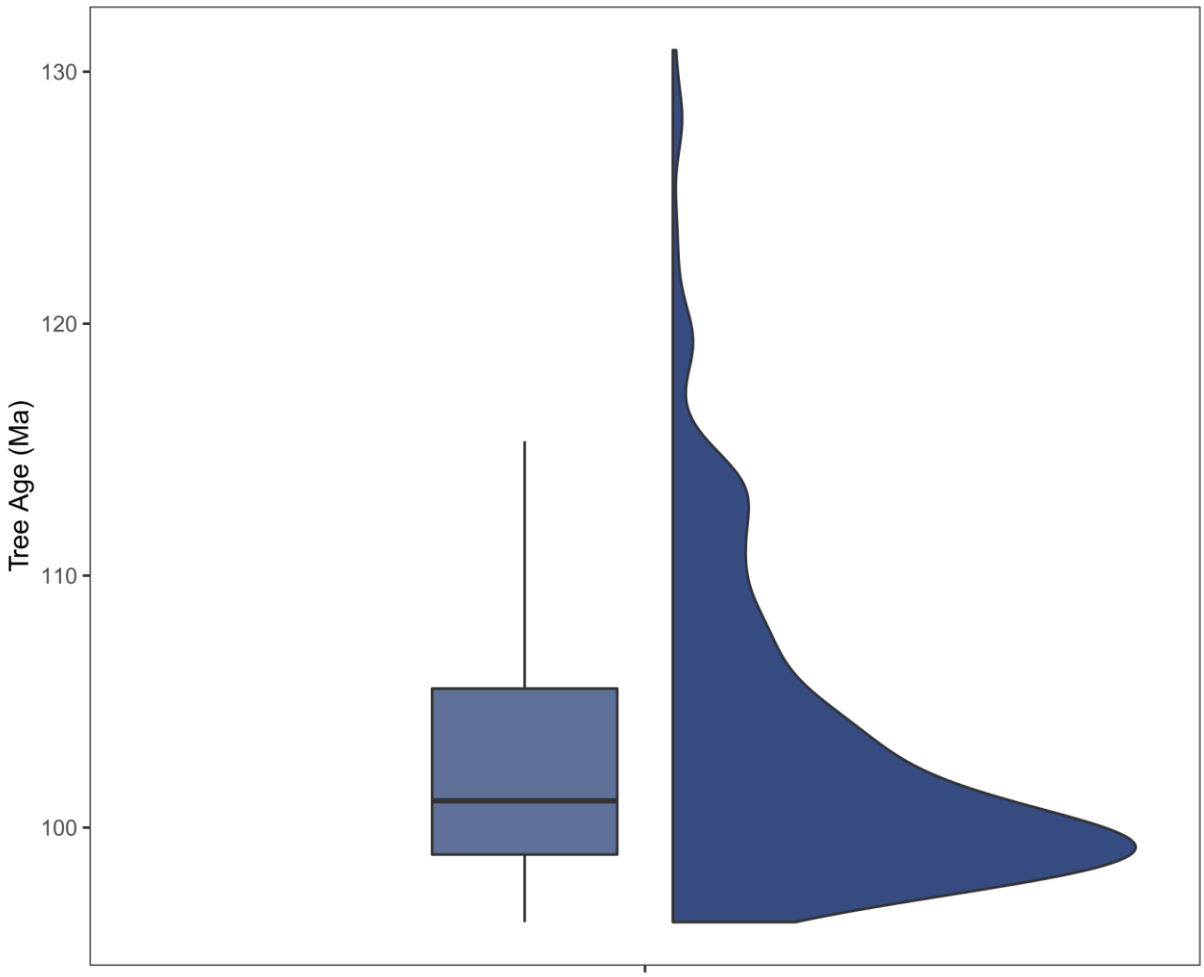

Fig. S11. Distribution plot showing the ages of 500 trees pulled from the posterior distribution. Tree ages range from 96.25 Ma to 130.86 Ma with a mean age of 103.18 Ma.

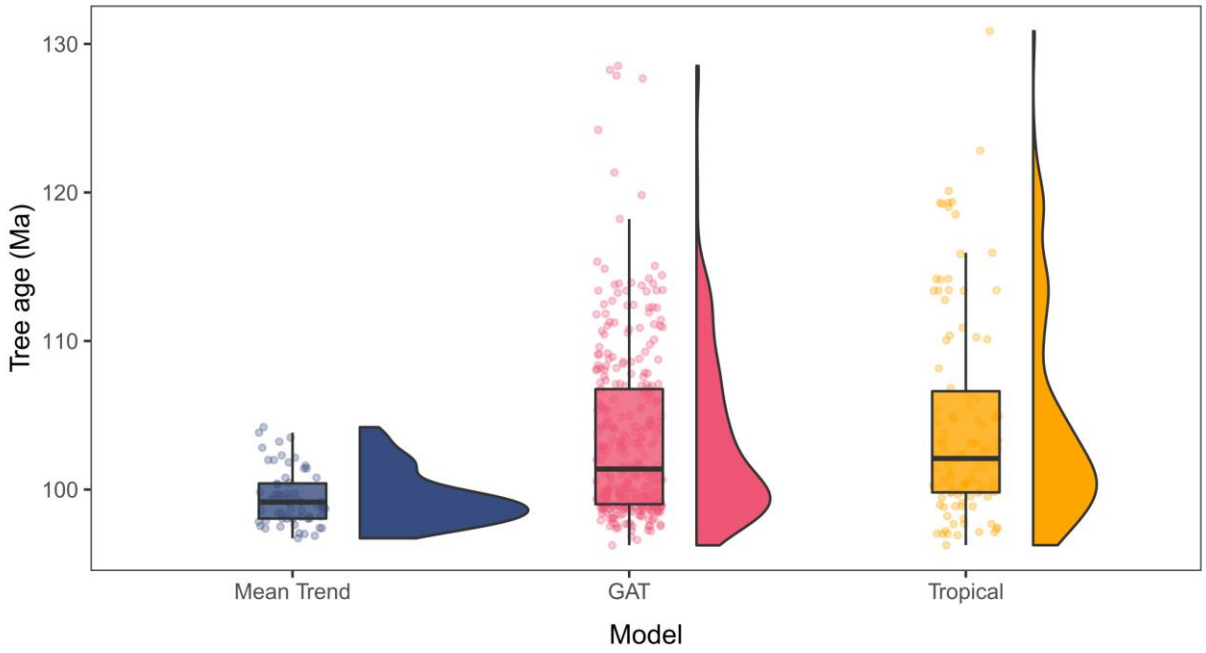

Fig. S12. Raincloud plots (half-violin plots and boxplots) showing the distribution of root ages of the 500 trees pulled from the posterior, separated by best-fit model.

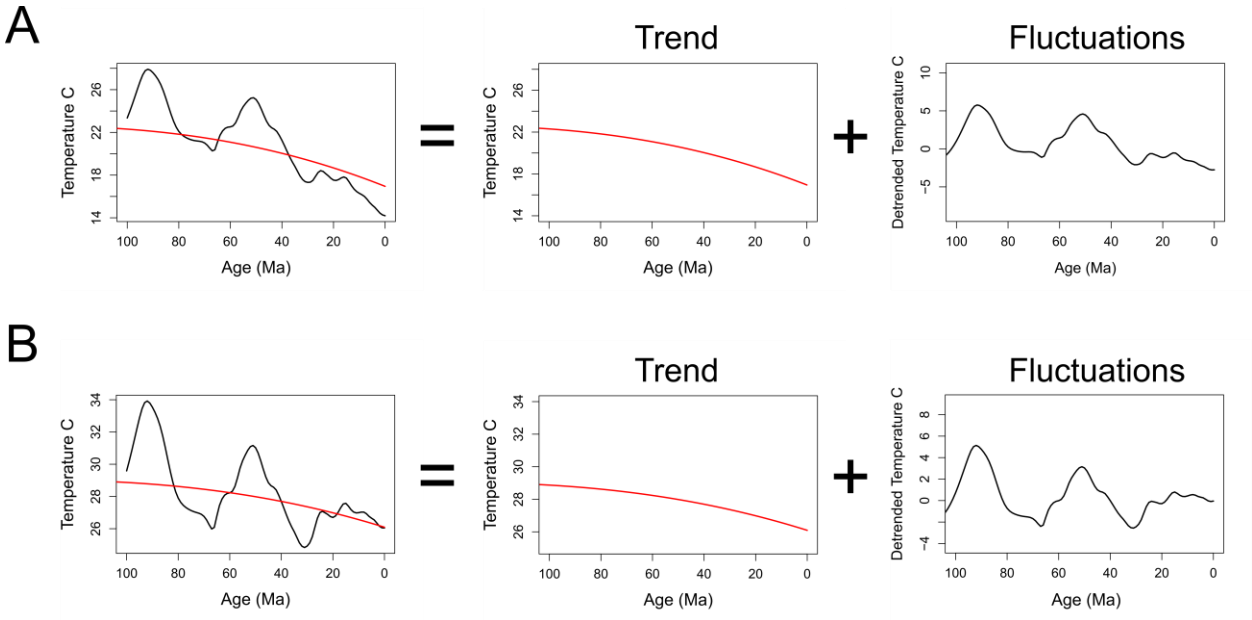

Fig. S13. The temperature curves for the **A)** global average temperature (GAT) and **B)** tropical latitude temperatures through the late Cretaceous to present day decomposed into an overall trend and the fluctuations around this trend. The temperature curve is thus the combination of the two curves.

A

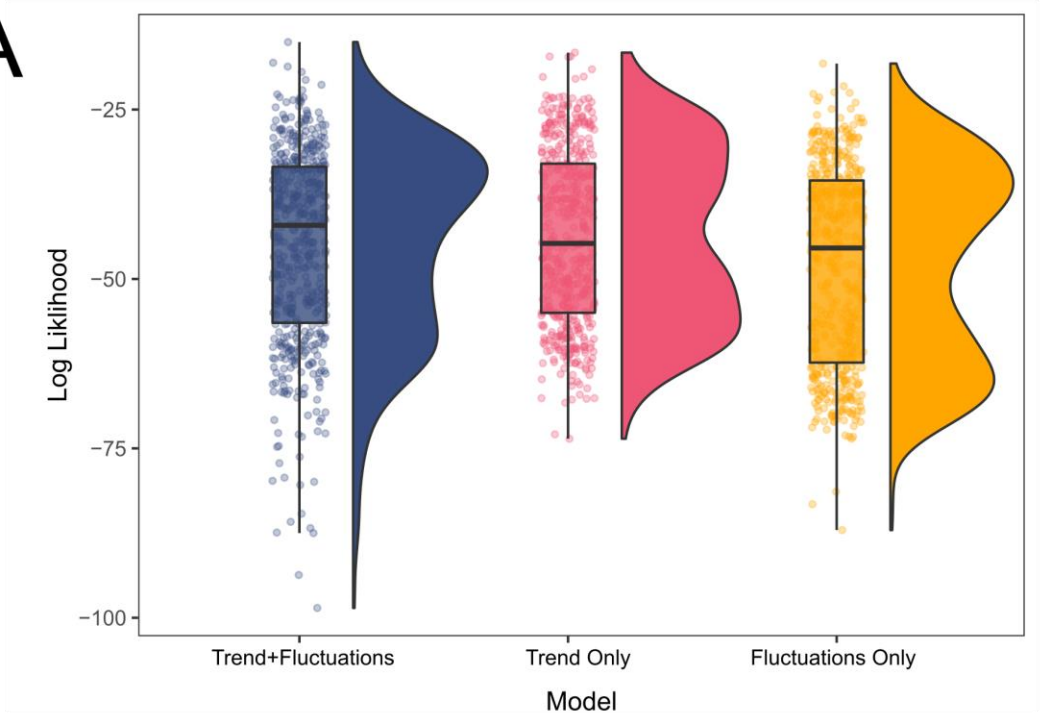
−25
−50
−75
−100
Log Liklihood
Trend+Fluctuations
Trend Only
Fluctuations Only
Model

B

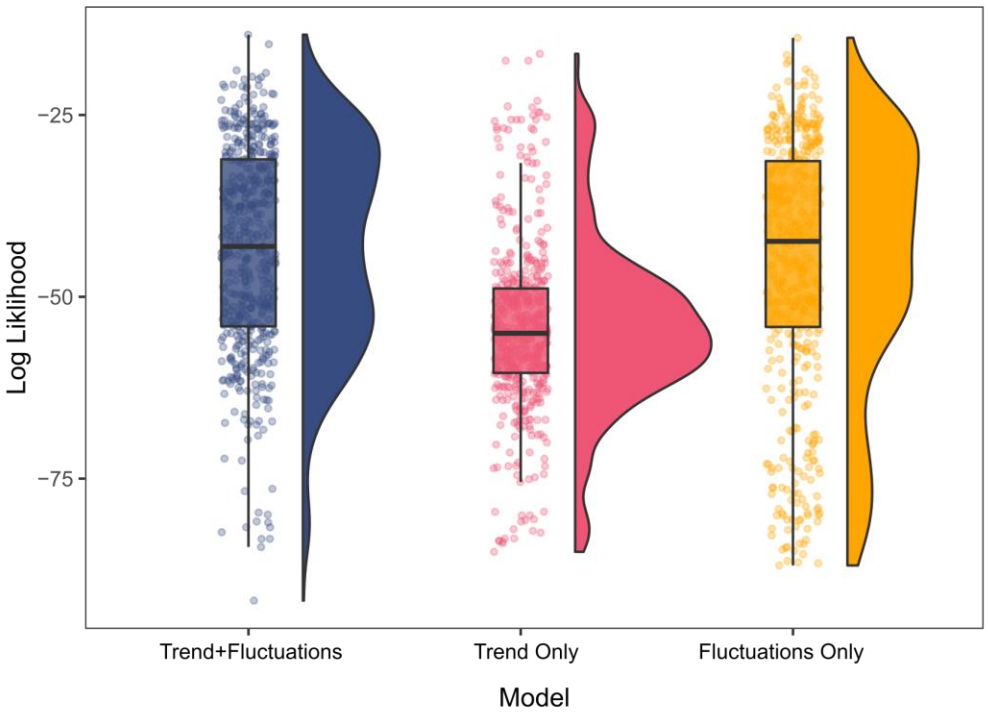
−25
−50
−75
Log Liklihood
Trend+Fluctuations
Trend Only
Fluctuations Only
Model

Fig. S14. Raincloud plots (half-violin plots and boxplots) of the decomposed OU climate models showing three tested models: both the overall global trend and the fluctuations around that trend, the trend only, and the fluctuations only. Figure displays the distribution of likelihood scores from 500 trees evenly selected from the posterior distribution of five independent gene subsets in the Bayesian analyses for **A)** the global average temperature (GAT) curve and **B)** the tropical latitude temperature curve.

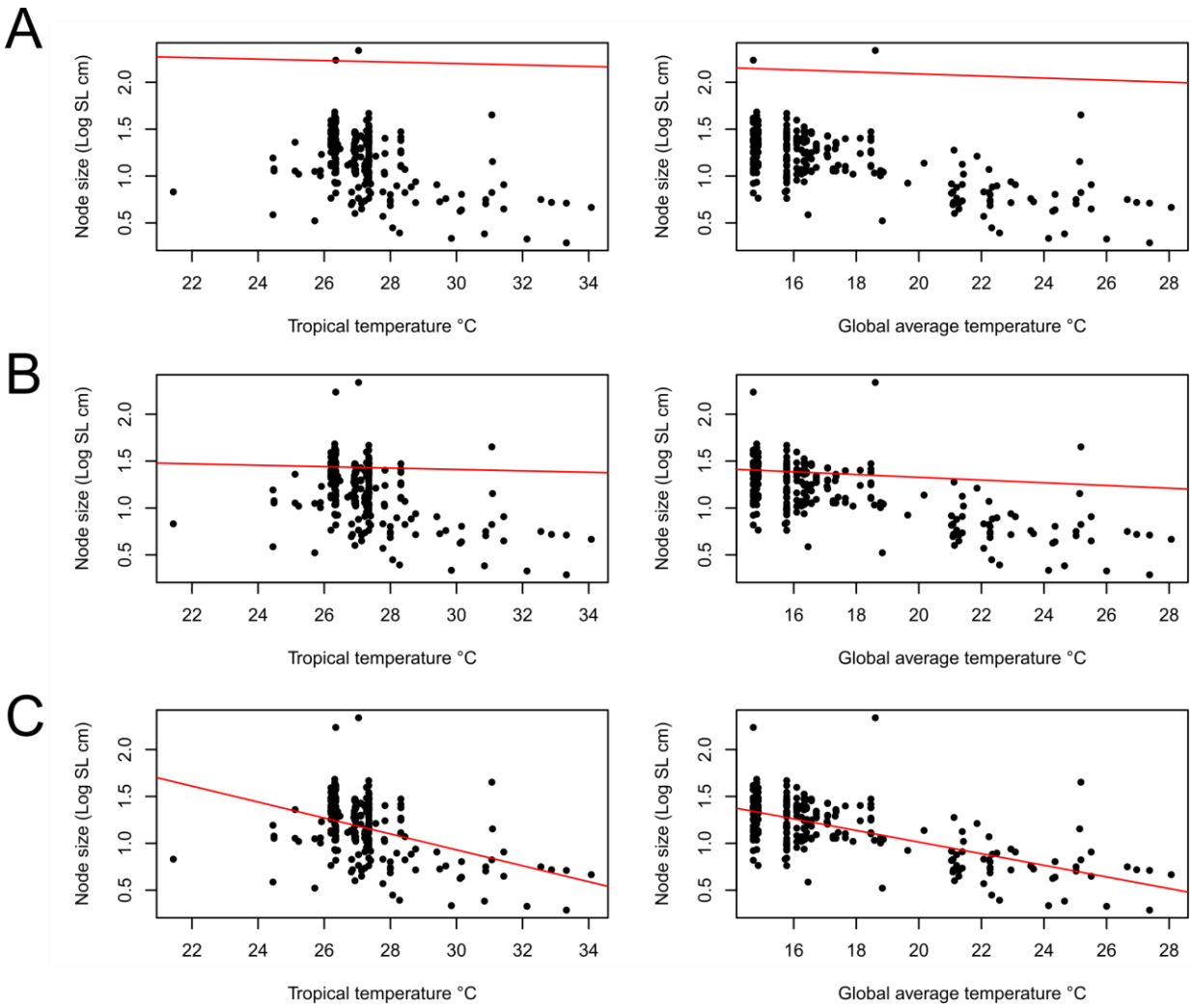

Fig. S15. Relationship between tetraodontiform body size and ocean temperature. Ancestral tetraodontiform body size, inclusive of superfamily Plectocretacicoidea, was reconstructed at each node in the maximum clade credibility tree and PGLS analyses under three different models: A) Ornstein-Uhlenbeck (OU) model, B) Brownian Motion (BM) model, and C) Ordinary Least Squares (OLS) model, were performed for two different curves: tropical (15°N-15°S) sea surface temperatures and global average sea temperatures. Under the best fit model (OU), Tetraodontiform body size is correlated with ocean temperatures using the global average curve (p = 5.571e-03) but not for the tropical curve (p =0. 0653).

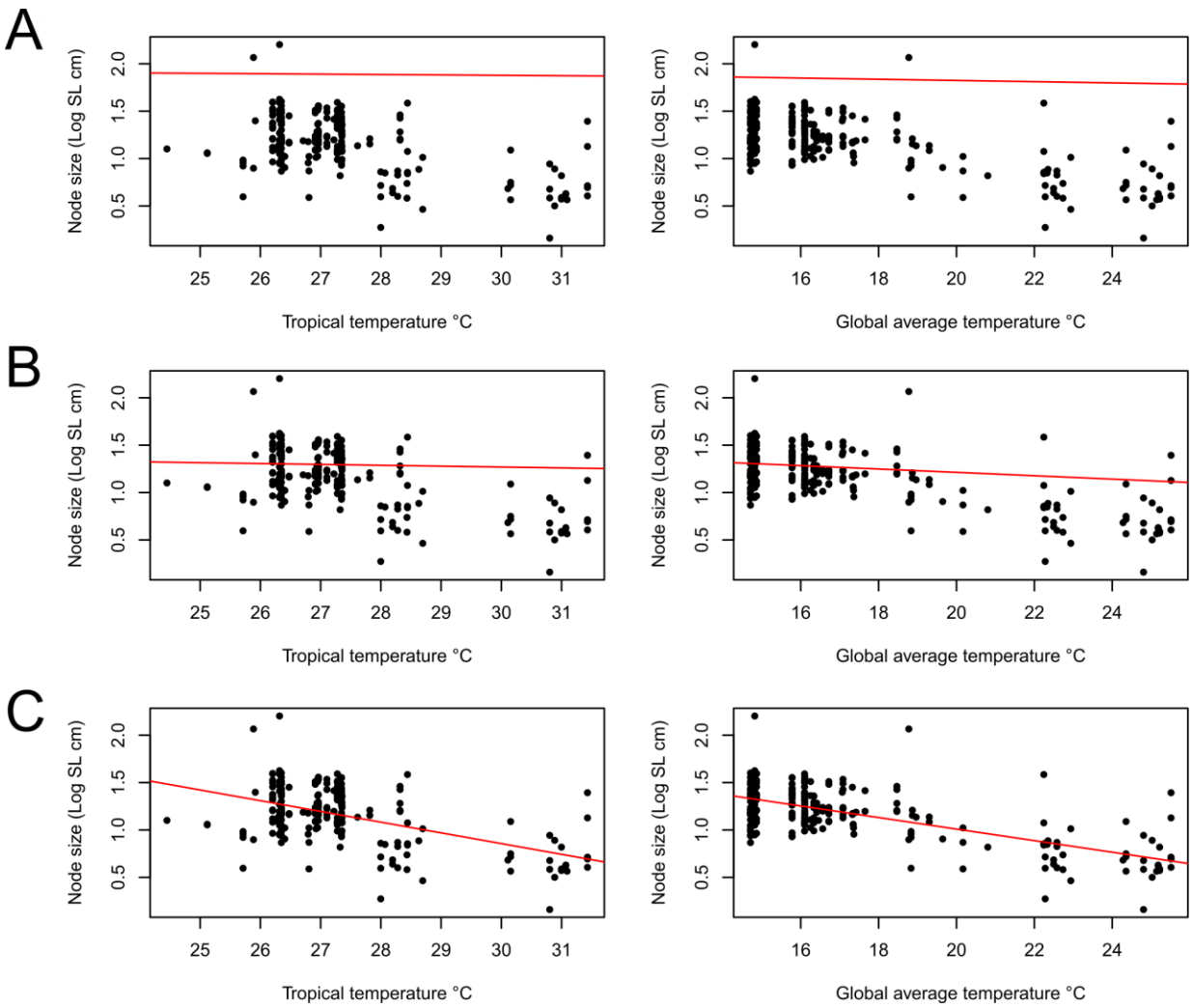

Fig. S16. Relationship between tetraodontiform body size and ocean temperature, without superfamily Plectocretacicoidea. Ancestral tetraodontiform body size, inclusive of superfamily Plectocretacicoidea, was reconstructed at each node in the maximum clade credibility tree and PGLS analyses under three different models: A) Ornstein-Uhlenbeck (OU) model, B) Brownian Motion (BM) model, and C) Ordinary Least Squares (OLS) model, were performed for two different curves: tropical (15°N-15°S) sea surface temperatures and global average sea temperatures (GAT). Under the best-fit model, Tetraodontiform body size is significantly correlated with GAT (BM model, p = 4.84e-05), but not tropical temperatures (OU model, p = 0.447).

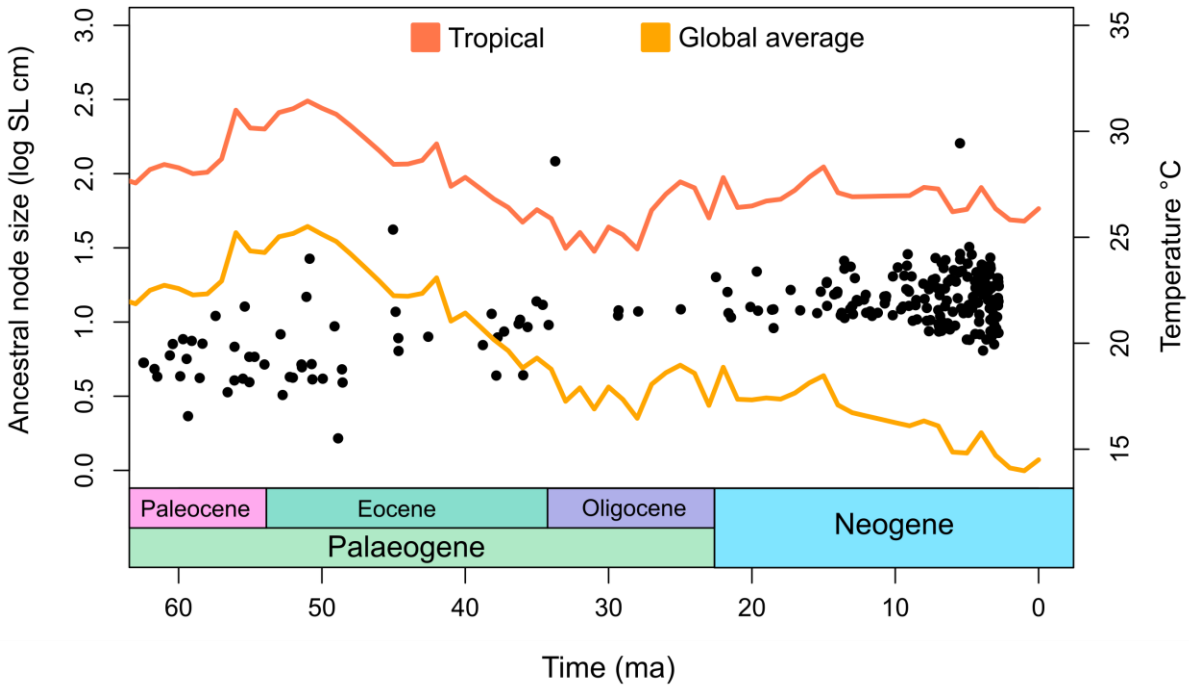

Fig. S17. Tetraodontiform body size and temperature over time, excluding Plectocretacicoidea. Sea surface temperature for tropical latitudes (15°N-15°S) (orange line) and a global average sea temperature (yellow line) are plotted for the past 63 Ma. The reconstructed ancestral node body size (log mean maximum standard length in cm) for tetraodontiforms is plotted in the same time scale. Sea temperatures have been slowly cooling over time, while tetraodontiform body size has been slowly increasing.

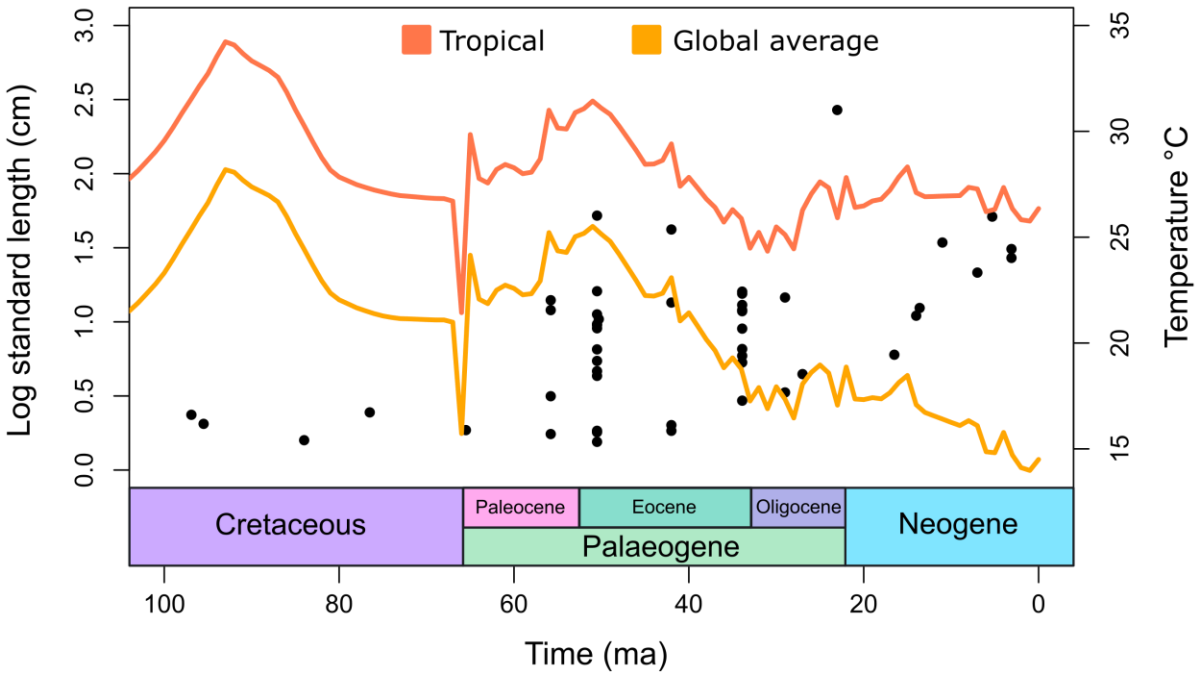

Fig. S18. Fossil tetraodontiform body size and temperature over time. Sea surface temperature for tropical latitudes (15°N-15°S) (orange line) and a global average sea temperature (yellow line) are plotted for the past 100 Ma. Body sizes for only fossil tetraodontiform species (log mean maximum standard length in cm) is plotted in the same time scale. Sea temperatures have been slowly cooling over time, while fossil tetraodontiform body size has been slowly increasing.

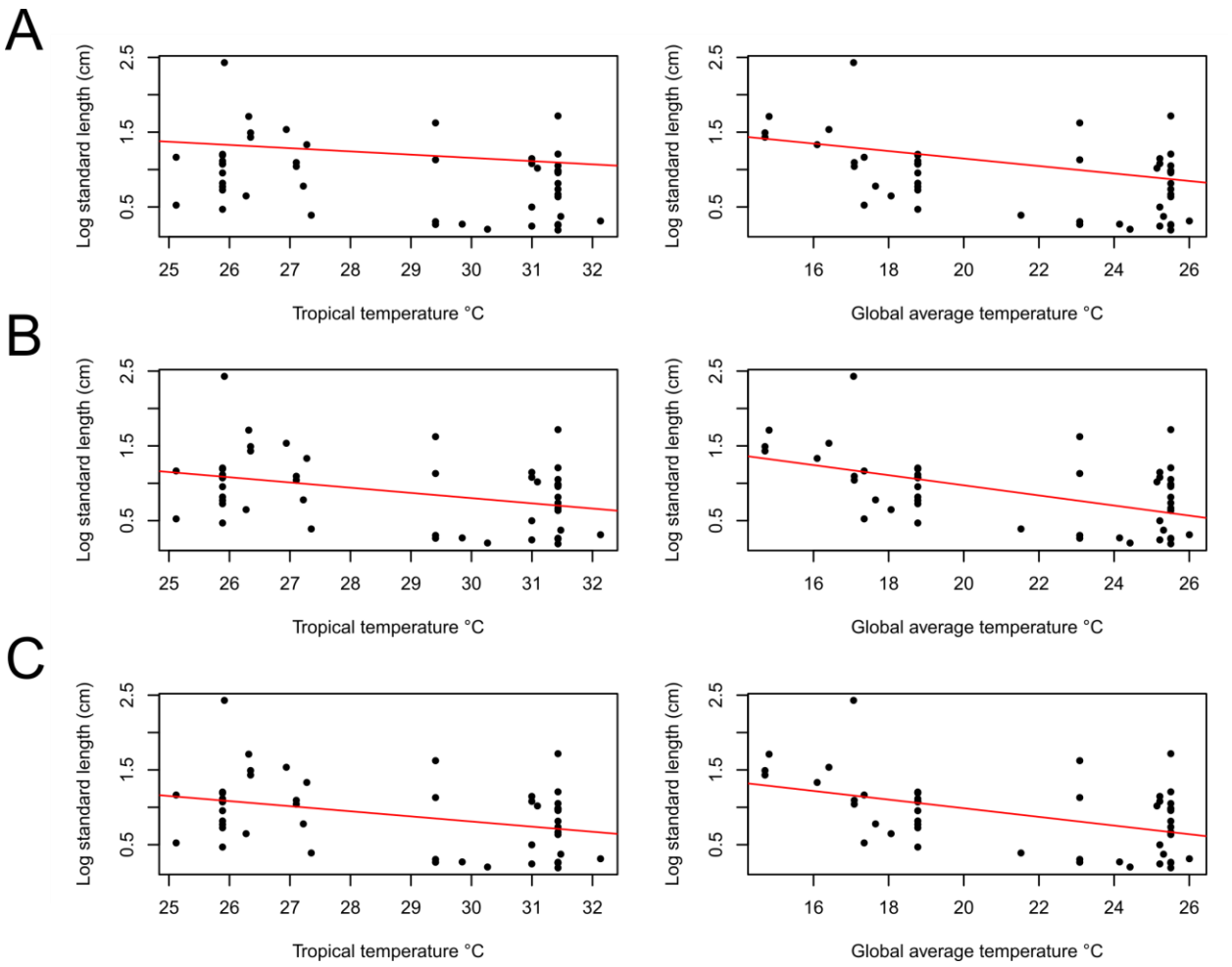

Fig. S19. Relationship between fossil tetraodontiform body size and ocean temperature. A PGLS analysis under three different models: A) Ornstein-Uhlenbeck (OU), B) Brownian Motion (BM), and C) Ordinary Least Squares (OLS) model, were performed between body size for fossil tetraodontiform species (log standard length (cm)) and ocean temperature for two different curves: tropical (15°N-15°S) sea surface temperatures and global average sea temperatures. Under the best fit model (OU), fossil body size is strongly correlated for global average temperature (p = 0.0311), but not tropical temperatures (p =0.1804).

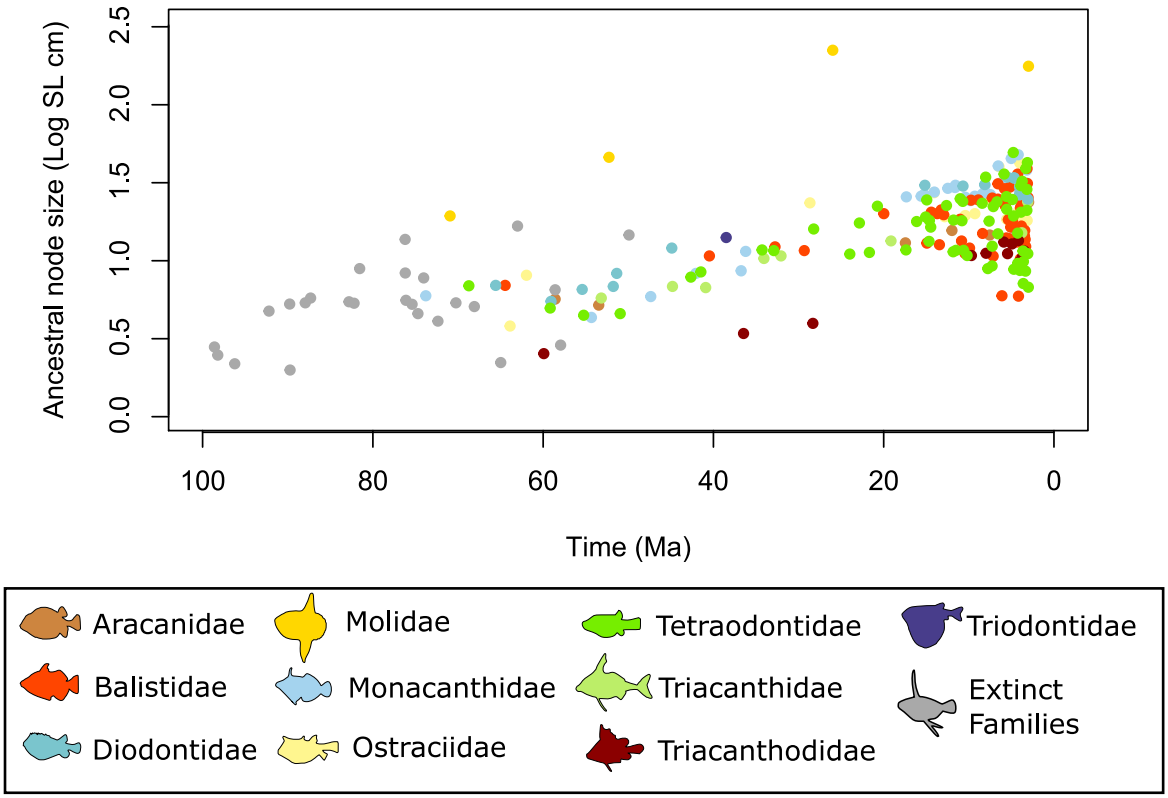

Fig. S20. Reconstructed ancestral node body size (log mean maximum standard length in cm) for tetraodontiforms is plotted against time. Nodal values are colored by family.

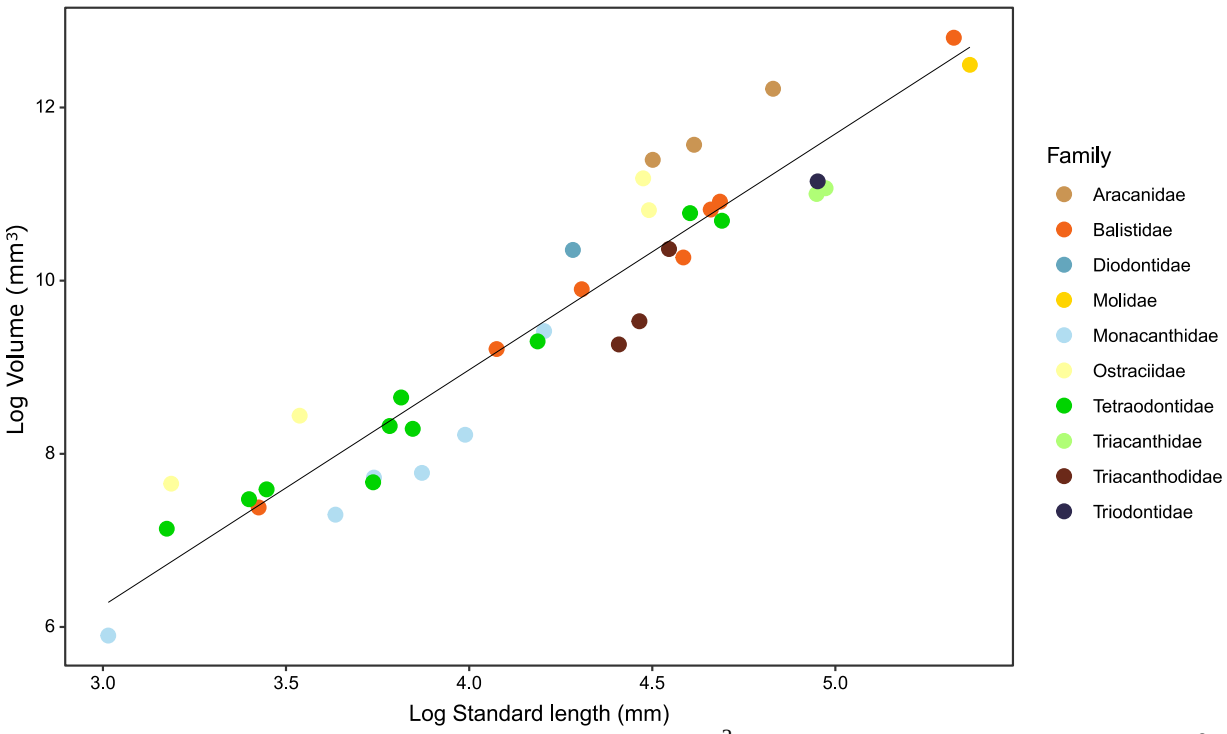

Fig. S21. Log standard length (mm) to log volume (mm^3) relationships between 41 species of tetraodontiform fishes across all 10 extant families. Data were collected from publicly available computed-tomography (CT) scan data accessed from MorphoSource.org as well as newly generated CT data. The image computing software Slicer was used to create three-dimensional models using CT data as input. Models were made solid using the WrapSolidify option to calculate volume. Standard length was measured using the ruler tool. A phylogenetic generalized least squares (PGLS) analysis shows the relationship between tetraodontiform standard length and volume is positively correlated ($p = 0.0005$).

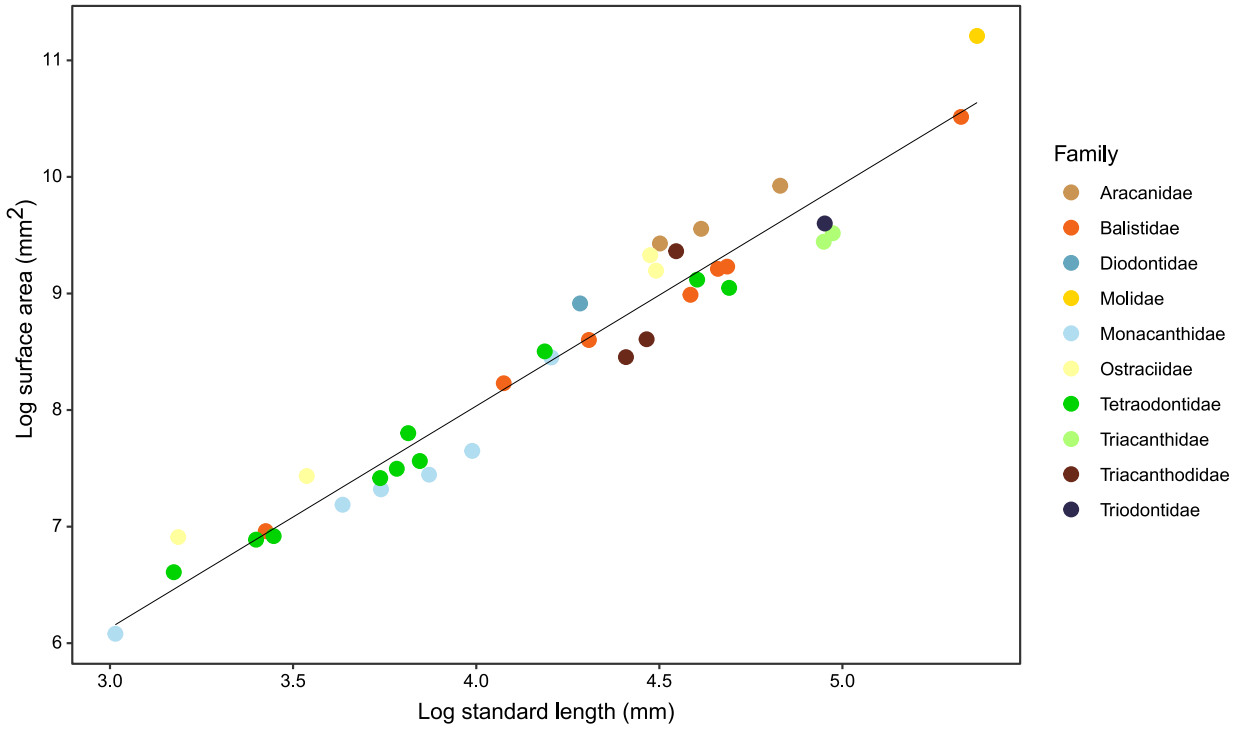

Fig. S22. Log standard length (mm) to log surface area (mm^2) relationships between 41 species of tetraodontiform fishes across all 10 extant families. Data were collected from publicly available computed-tomography (CT) scan data accessed from MorphoSource.org as well as newly generated CT data. The image computing software Slicer was used to create three-dimensional models using CT data as input. Models were made solid using the WrapSolidify option to calculate surface area. Standard length was measured using the ruler tool. A phylogenetic generalized least squares (PGLS) analysis shows the relationship between tetraodontiform standard length and volume is positively correlated ($p = 0.0248$).

Table S1. Summary of tree age prior effect on the root node (Tetraodontiformes+Outgroups). Table indicates the root prior distribution (offset exponential or uniform), whether or not the analysis ran with data, and a summary of the 95% highest posterior density (HPD) values for the mean root age, root age variance, upper and lower age bounds, and median root age. Bounds for the offset exponential root distribution were a minimum age of 95 Ma and a mean age of 107.9 Ma. Bounds for the uniform root distribution were a minimum age of 95.9 Ma and maximum age of 110 Ma.

				95% HPD Interval		
Root Distribution	**With data?**	**Mean**	**Variance**	**Lower**	**Upper**	**Median**
Offset Exponential	Yes	132.3739	204.7114	111.412	161.6181	129.3902
Offset Exponential	No	112.5834	55.90838	99.3592	126.3776	111.5328
Uniform	Yes	108.9578	0.964899	107.2127	110	109.267
Uniform	No	106.3641	6.494229	101.5038	109.9977	106.7817

Table S2. Summary of tree age prior effect on the root node (Tetraodontiformes+Outgroups) when Plectocretacicoidea is excluded. Table indicates the root prior distribution (offset exponential or uniform), whether or not the analysis ran with data, and a summary of the 95% highest posterior density (HPD) values for the mean root age, root age variance, upper and lower age bounds, and median root age. Bounds for the offset exponential root distribution were a minimum age of 59 Ma and a mean age of 61.8 Ma. Bounds for the uniform root distribution were a minimum age of 59 Ma and maximum age of 67.43 Ma

				95% HPD Interval		
Root Distribution	**With data?**	**Mean**	**Variance**	**Lower**	**Upper**	**Median**
Offset Exponential	Yes	93.30206	85.84346	73.55835	110.9355	92.23749
Offset Exponential	No	74.26792	19.14679	66.2045	82.83702	73.96716
Uniform	Yes	67.15891	0.07243	66.53637	67.42502	67.25915
Uniform	No	66.48487	0.714063	64.6329	67.42978	66.73349

Table S3. Summary of tree age prior effect on the crown node (crown Tetraodontiformes). Table indicates the root prior distribution (offset exponential or uniform), whether or not the analysis ran with data, and a summary of the 95% highest posterior density (HPD) values for the mean crown age, crown age variance, upper and lower age bounds, and median crown age. No age priors were placed onto the node for crown Tetraodontiformes.

				95% HPD Interval		
Root Distribution	**With data?**	**Mean**	**Variance**	**Lower**	**Upper**	**Median**
Offset Exponential	Yes	99.8399	49.56933	84.2824	112.6877	100.0196
Offset Exponential	No	94.55334	55.47974	79.4895	108.6024	94.97438
Uniform	Yes	94.72298	11.65628	87.54332	100.2006	95.3393
Uniform	No	92.28921	43.32038	79.27937	103.7278	92.94941

Table S4. Summary of tree age prior effect on the crown node (crown Tetraodontiformes) when Plectocretacicoidea is excluded. Table indicates the root prior distribution (offset exponential or uniform), whether or not the analysis ran with data, and a summary of the 95% highest posterior density (HPD) values for the mean crown age, crown age variance, upper and lower age bounds, and median crown age. No age priors were placed onto the node for crown Tetraodontiformes.

				95% HPD Interval		
Root Distribution	**With data?**	**Mean**	**Variance**	**Lower**	**Upper**	**Median**
Offset Exponential	Yes	80.66592	42.09142	67.29957	93.55297	79.65927
Offset Exponential	No	71.04824	13.99969	64.13806	78.6117	70.88791
Uniform	Yes	62.45651	1.159584	60.80456	64.29212	62.4217
Uniform	No	65.11428	1.201485	62.871	66.96123	65.25346

Table S5. Evolutionary model results, including the deep-sea temperature curve from Cramer et al. 2011 (33). Number of model parameters, mean values for the corrected Akaike information criterion (AICc), mean log likelihood (lnL), and weighted AIC (AICw) are reported.

Evolutionary Model	Parameters	AICc	lnL	AICw
OU climate deep-sea	5	89.87	-39.81	0.9849
OU climate GAT	5	98.25	-43.99	0.0149
OU climate tropical	5	112.42	-51.08	1.25e-05
Mean trend	3	126.91	-60.40	8.95e-09
OU	3	137.88	-65.89	3.71e-11
Rate trend	3	146.78	-70.34	4.33e-13
BM	2	148.01	-71.98	2.34e-13
EB	3	148.03	-70.96	2.31e-13

Table S6. **Evolutionary model results, excluding superfamily Plectocretacicoidea.** Model fitting results for the seven macroevolutionary models tested. Models were tested on 500 trees selected from the combined posterior distributions of five gene subsets. Number of model parameters and mean values for the corrected Akaike information criterion (AICc), log likelihood (lnL), and weighted AIC (AICw) are reported. The strongest support went to the climate-driven model using the global average temperature curve.

Evolutionary Model	Parameters	AICc	lnL	AICw
OU climate GAT	5	111.51	-50.62	0.996
OU climate tropical	5	122.52	-56.13	4.04e-03
OU	3	141.92	-67.91	2.47e-07
Mean trend	3	149.42	-71.66	5.82e-09
EB	3	165.91	-79.90	1.53e-12
Rate trend	3	166.55	-80.22	1.11e-12
BM	2	169.80	-82.87	2.18e-13

Table S7. Number of times each evolutionary model was the best fit. Summary of the best fitting evolutionary model for each of the 500 trees selected from the posterior distribution of the Bayesian analysis, for both fossil schemes (with/without superfamily Plectocretacicoidea). The best fit model for each of the 500 trees was determined from the highest weighted Akaike information criterion (AICw) score. The OU climate model using the global average temperature (GAT) curve was the best fitting model overall (329/500 trees; 65.8%) for the scheme inclusive of the superfamily Plectocretacicoidea and also for the scheme excluding them (395/500 trees; 79%).

	Number of trees (%)	
Evolutionary Model	**With Plectocretacicoidea**	**Without Plectocretacicoidea**
OU climate GAT	329 (65.8%)	395 (79%)
OU climate tropical	107 (21.4 %)	102 (20.4%)
Mean trend	64 (12.8%)	3 (0.006%)
OU	0 (0%)	0 (0%)
Rate trend	0 (0%)	0 (0%)
BM	0 (0%)	0 (0%)
EB	0 (0%)	0 (0%)

Table S8. Decomposed climate OU model fitting results for the global average temperature curve (GAT). Number of model parameters, mean values for corrected Akaike information criterion (AICc), mean log likelihood (lnL), and weighted AICc (AICw) are reported. Most model support went to a temperature curve composed of a trend parameter and a fluctuations parameter.

Model	Parameters	AICc	lnL	AICw
Trend+Fluctuations	6	96.53	-42.08	0.7697
Trend	5	99.77	-44.75	0.1524
Fluctuations	5	101.12	-45.43	0.0777

Table S9. Decomposed climate OU model fitting results for the tropical latitude temperature curve. Number of model parameters, mean values for corrected Akaike information criterion (AICc), mean log likelihood (lnL), and weighted AICc (AICw) are reported. Most model support went to a temperature curve composed of only the fluctuations parameter.

Model	Parameters	AICc	lnL	AICw
Fluctuations	5	95.01	-42.37	0.8522
Trend+Fluctuations	6	98.52	-43.07	0.1477
Trend	5	120.29	-55.01	2.77e-06

Table S10. PGLS model fitting results, including superfamily Plectocretacicoidea. Model fitting results for two temperature curves (global average temperature (GAT) and tropical latitudes) for phylogenetic generalized least squares (PGLS) analyses under an Ornstein-Uhlenbeck (OU) model, a Brownian Motion (BM) model, and a model where phylogeny is not considered (i.e. Ordinary Least Squares (OLS)). The Akaike information criterion (AIC), log likelihood (lnL) and p values are reported for each model. Highest support went to an OU model for both temperature curves.

Temperature curve	Model	AIC	lnL	p value
GAT	OU	-480.584	244.292	5.571E-03
GAT	BM	-452.838	229.418	4.51E-04
GAT	OLS	-2.9266	4.463	2.56E-29
Tropical	OU	-476.312	242.156	6.54E-02
Tropical	BM	-442.797	224.3984	1.23E-01
Tropical	OLS	81.05182	-37.5259	4.76E-11

Table S11. PGLS model fitting results, excluding superfamily Plectocretacicoidea. Model fitting results for two temperature curves (global average temperature (GAT) and tropical latitudes) for phylogenetic generalized least squares (PGLS) analyses under an Ornstein-Uhlenbeck (OU) model, a Brownian Motion (BM) model, and a model where phylogeny is not considered (i.e. Ordinary Least Squares (OLS)). The Akaike information criterion (AIC), log likelihood (lnL) and p values are reported for each model. Highest support went to a BM model for the GAT curve and an OU model for the tropical curve.

Temperature curve	Model	AIC	lnL	p value
GAT	OU	-476.94	242.470	0.208
GAT	BM	-488.651	247.325	4.84E-05
GAT	OLS	-38.771	22.385	1.82E-31
Tropical	OU	-475.923	241.961	0.447
Tropical	BM	-474.703	240.352	0.0995
Tropical	OLS	25.211	-9.605	1.37E-17

Table S12. PGLS model fitting results for only fossil Tetraodontiformes. Model fitting results for two temperature curves (global average temperature (GAT) and tropical latitudes) for phylogenetic generalized least squares (PGLS) analyses under an Ornstein-Uhlenbeck (OU) model, a Brownian Motion (BM) model, and a model where phylogeny is not considered (i.e. Ordinary Least Squares (OLS)). The Akaike information criterion (AIC), log likelihood (lnL) and p values are reported for each model. Highest support went to an OU model for both temperature curves.

Temperature curve	Model	AIC	lnL	p value
GAT	OU	48.627	-20.313	0.0311
GAT	BM	51.578	-22.789	1.53E-03
GAT	OLS	60.689	-27.344	7.53E-04
Tropical	OU	51.543	-21.771	0.1804
Tropical	BM	56.779	-25.389	0.0239
Tropical	OLS	66.134	-30.067	0.0128

Table S13. List of specimens newly sequenced (141 Tetraodontiformes representing 131 unique species) and four outgroup Lophiiformes). The museum catalog tissue and voucher numbers are provided. One specimen (*Rhinecanthus verrucosus*) was excluded from the analyses due to low capture efficiency and only being represented in a single gene.

Affiliation	Family	Species Name	Voucher Number	Tissue Collection Number
Outgroup	Lophiidae	*Lophiodes caulinaris*	USNM 421345	USNM AG7PC44
Outgroup	Lophiidae	*Lophiodes spilurus*	USNM 421229	USNM AG7PF91
Outgroup	Lophiidae	*Lophiomus setigerus*	CSIRO H 6570-04	CSIRO GT 1833
Outgroup	Lophiidae	*Lophius litulon*	CSIRO H 7394-66	CSIRO GT 6889
Eupercaria	Aracanidae	*Anoplocapros amygdaloides*	CSIRO H 6351-13	CSIRO GT 5967
Eupercaria	Aracanidae	*Anoplocapros inermis*	CSIRO H 6836-11	CSIRO GT 3695
Eupercaria	Aracanidae	*Anoplocapros lenticularis*	CSIRO H 6341-11	CSIRO GT 214
Eupercaria	Aracanidae	*Aracana aurita*	CSIRO H 6812-01	CSIRO GT 2350
Eupercaria	Aracanidae	*Caprichthys gymnura*	CSIRO H 6341-02	CSIRO GT 203
Eupercaria	Aracanidae	*Capropygia unistriata*	CSIRO H 6350-23	CSIRO GT 5956
Eupercaria	Balistidae	*Abalistes filamentosus*	CSIRO unreg LM964	CSIRO IN02982
Eupercaria	Balistidae	*Balistes capriscus*	USNM 405175	USNM AD9NF67
Eupercaria	Balistidae	*Balistes polylepis*	USNM 421241	USNM AG7PC77
Eupercaria	Balistidae	*Balistes vetula*	No voucher	UPRFL0353
Eupercaria	Balistidae	*Balistoides viridescens*	USNM 403379	USNM AG9RF59
Eupercaria	Balistidae	*Canthidermis sufflamen*	USNM 423028	USNM AC7BZ85
Eupercaria	Balistidae	*Melichthys niger*	No voucher	UPRFL0061
Eupercaria	Balistidae	*Melichthys vidua*	STRI-X-60	STRI BFT11786
Eupercaria	Balistidae	*Odonus niger*	USNM 409200	USNM AG7PW08
Eupercaria	Balistidae	*Pseudobalistes fuscus*	USNM 400523	USNM AG9RP93
Eupercaria	Balistidae	*Rhinecanthus aculeatus*	USNM 400511	USNM AG9RU13
Eupercaria	Balistidae	*Rhinecanthus lunula*	USNM 392212	USNM AG5NP92
Eupercaria	Balistidae	*Rhinecanthus rectangulus*	USNM 400515	USNM AG9RQ72
Eupercaria	Balistidae	*Rhinecanthus verrucosus*	USNM 435559	USNM AB6QS48
Eupercaria	Balistidae	*Sufflamen bursa*	USNM 392517	USNM AG5NQ79
Eupercaria	Balistidae	*Sufflamen chrysopterum*	AMS I.44740-006	CSIRO UG0735
Eupercaria	Balistidae	*Sufflamen chrysopterum*	USNM 435999	USNM AC1VD99
Eupercaria	Balistidae	*Xanthichthys auromarginatus*	USNM 409459	USNM AG7PY24
Eupercaria	Balistidae	*Xanthichthys caeruleolineatus*	USNM 409149	USNM AG7PV58
Eupercaria	Balistidae	*Xanthichthys caeruleolineatus*	CSIRO H 6318-01	CSIRO GT 168
Eupercaria	Balistidae	*Xanthichthys lineopunctatus*	CSIRO unreg KD795	CSIRO IN02440
Eupercaria	Diodontidae	*Chilomycterus antennatus*	USNM 414367	USNM AC2WT95
Eupercaria	Diodontidae	*Chilomycterus reticulatus*	CSIRO H 7305-08	CSIRO IN02878
Eupercaria	Diodontidae	*Chilomycterus schoepfii*	USNM 415605	USNM AC2WQ63
Eupercaria	Diodontidae	*Chilomycterus spinosus*	USNM 405184	USNM AD9NF85
Eupercaria	Diodontidae	*Diodon holocanthus*	No voucher	UPRFL0286
Eupercaria	Diodontidae	*Diodon hystrix*	STRI-X-325	STRI BFT11552
Eupercaria	Diodontidae	*Diodon nicthemerus*	CSIRO H 6347-31	CSIRO GT 5963
Eupercaria	Diodontidae	*Tragulichthys jaculiferus*	CSIRO unreg	CSIRO GT 4734

Eupercaria	Monacanthidae	*Acanthaluteres spilomelanurus*	CSIRO H 7101-12	CSIRO GT 5571
Eupercaria	Monacanthidae	*Acanthaluteres vittiger*	CSIRO H 6945-04	CSIRO GT 4819
Eupercaria	Monacanthidae	*Aluterus heudelotii*	USNM 405092	USNM AD9NE01
Eupercaria	Monacanthidae	*Aluterus monoceros*	No voucher	UPRFL1497
Eupercaria	Monacanthidae	*Aluterus scriptus*	No voucher	UPRFL0003
Eupercaria	Monacanthidae	*Amanses scopas*	USNM 392430	USNM AG5NQ54
Eupercaria	Monacanthidae	*Anacanthus barbatus*	CSIRO H 6146-06	CSIRO GT 4577
Eupercaria	Monacanthidae	*Brachaluteres jacksonianus*	CSIRO H 7103-08	CSIRO GT 5588
Eupercaria	Monacanthidae	*Brachaluteres taylori*	CSIRO H 6914-01	CSIRO GT 4430
Eupercaria	Monacanthidae	*Cantherhines dumerilii*	USNM 399512	USNM AG9RT41
Eupercaria	Monacanthidae	*Cantherhines fronticinctus*	USNM 436443	USNM AC1VI44
Eupercaria	Monacanthidae	*Cantherhines longicaudus*	USNM 400537	USNM AG9RP49
Eupercaria	Monacanthidae	*Cantherhines nukuhiva*	USNM 409267	USNM AG7PW33
Eupercaria	Monacanthidae	*Cantherhines pardalis*	USNM 435717	USNM AB6QU07
Eupercaria	Monacanthidae	*Cantherhines pullus*	No voucher	UPRFL0403
Eupercaria	Monacanthidae	*Cantherhines sandwichiensis*	USNM 392012	USNM AG5NP68
Eupercaria	Monacanthidae	*Cantheschenia grandisquamis*	CSIRO unreg	CSIRO GT 4763
Eupercaria	Monacanthidae	*Chaetodermis penicilligerus*	CSIRO H 6911-05	CSIRO GT 4402
Eupercaria	Monacanthidae	*Chaetodermis penicilligerus*	CSIRO H 8251-01	CSIRO GT 10694
Eupercaria	Monacanthidae	*Eubalichthys bucephalus*	Not retained	CSIRO GT 216
Eupercaria	Monacanthidae	*Eubalichthys caeruleoguttatus*	CSIRO H 8282-02	CSIRO GT 10791
Eupercaria	Monacanthidae	*Eubalichthys gunnii*	CSIRO H 6944-01	CSIRO GT 4806
Eupercaria	Monacanthidae	*Eubalichthys mosaicus*	CSIRO H 6350-07	CSIRO GT 5914
Eupercaria	Monacanthidae	*Eubalichthys quadrispinis*	CSIRO H 6348-07	CSIRO GT 311
Eupercaria	Monacanthidae	*Meuschenia trachylepis*	CSIRO H 6838-09	CSIRO GT 3654
Eupercaria	Monacanthidae	*Oxymonacanthus longirostris*	AMS I.44739-002	CSIRO UG0755
Eupercaria	Monacanthidae	*Paramonacanthus choirocephalus*	CSIRO H 6145-06	CSIRO GT 4410
Eupercaria	Monacanthidae	*Paramonacanthus filicauda*	CSIRO H 6319-07	CSIRO GT 4617
Eupercaria	Monacanthidae	*Paramonacanthus japonicus*	CSIRO unreg BY011	CSIRO IN00550
Eupercaria	Monacanthidae	*Paramonacanthus lowei*	CSIRO unreg	CSIRO CMR005207a
Eupercaria	Monacanthidae	*Paramonacanthus lowei*	CSIRO unreg	CSIRO CMR005207b
Eupercaria	Monacanthidae	*Paramonacanthus oblongus*	CSIRO unreg	CSIRO GT 4244
Eupercaria	Monacanthidae	*Pervagor aspricaudus*	USNM 390982	USNM AG5NP14
Eupercaria	Monacanthidae	*Pervagor janthinosoma*	AMS I.44714-026	CSIRO UG0193
Eupercaria	Monacanthidae	*Pervagor marginalis*	USNM 409029	USNM AG7PU39
Eupercaria	Monacanthidae	*Pervagor melanocephalus*	USNM 435755	USNM AB6QU45
Eupercaria	Monacanthidae	*Pseudalutarius nasicornis*	CSIRO H 6937-08	CSIRO GT 4711
Eupercaria	Monacanthidae	*Pseudomonacanthus elongatus*	CSIRO H 6904-02	CSIRO GT 4289
Eupercaria	Monacanthidae	*Pseudomonacanthus elongatus*	CSIRO H 8249-02	CSIRO GT 10812
Eupercaria	Monacanthidae	*Pseudomonacanthus macrurus*	USNM 435396	USNM AB6QQ85
Eupercaria	Monacanthidae	*Pseudomonacanthus peroni*	CSIRO H 4643-03	CSIRO 10V
Eupercaria	Monacanthidae	*Rudarius minutus*	WAM P.33523-001	CSIRO UG0547
Eupercaria	Monacanthidae	*Stephanolepis hispidus*	USNM 405062	USNM AD9ND41
Eupercaria	Monacanthidae	*Stephanolepis setifer*	USNM 419328	USNM AC4YM29
Eupercaria	Monacanthidae	*Thamnaconus degeni*	CSIRO H 6942-04	CSIRO GT 4786
Eupercaria	Monacanthidae	*Thamnaconus striatus*	CSIRO H 7220-09	CSIRO IN02545

Eupercaria	Monacanthidae	*Thamnaconus tessellatus*	CSIRO H 6422-04	CSIRO GT 715
Eupercaria	Ostraciidae	*Acanthostracion polygonius*	USNM 421721	USNM AC2WV43
Eupercaria	Ostraciidae	*Acanthostracion quadricornis*	No voucher	UPRFL0075
Eupercaria	Ostraciidae	*Lactophrys trigonus*	USNM 415636	USNM AC2WQ88
Eupercaria	Ostraciidae	*Lactophrys triqueter*	No voucher	UPRFL0225
Eupercaria	Ostraciidae	*Lactophrys triqueter*	No voucher	UPRFL0072
Eupercaria	Ostraciidae	*Lactoria cornuta*	USNM 403207	USNM AG9RD87
Eupercaria	Ostraciidae	*Ostracion cubicus*	USNM 391997	USNM AG5NP65
Eupercaria	Ostraciidae	*Ostracion meleagris*	USNM 400508	USNM AG9RT93
Eupercaria	Ostraciidae	*Ostracion nasus*	CSIRO unreg	CSIRO GT 4682
Eupercaria	Ostraciidae	*Ostracion whitleyi*	USNM 409290	USNM AG7PW56
Eupercaria	Tetraodontidae	*Arothron hispidus*	USNM 400510	USNM AG9RU11
Eupercaria	Tetraodontidae	*Arothron hispidus*	CSIRO H 8228-02	CSIRO GT 10604
Eupercaria	Tetraodontidae	*Arothron meleagris*	USNM 391239	USNM AG5NP43
Eupercaria	Tetraodontidae	*Arothron nigropunctatus*	NMV A.29880-008	CSIRO UG0991
Eupercaria	Tetraodontidae	*Canthigaster axiologus*	USNM 400503	USNM AG9RT89
Eupercaria	Tetraodontidae	*Canthigaster bennetti*	USNM 439632	USNM AG5NT52
Eupercaria	Tetraodontidae	*Canthigaster criobe*	USNM 400521	USNM AG9RL45
Eupercaria	Tetraodontidae	*Canthigaster cyanospilota*	CSIRO H 8206-01	CSIRO GT 10464
Eupercaria	Tetraodontidae	*Canthigaster janthinoptera*	USNM 392325	USNM AG5NQ15
Eupercaria	Tetraodontidae	*Canthigaster marquesensis*	USNM 409458	USNM AG7PY23
Eupercaria	Tetraodontidae	*Canthigaster punctatissima*	No voucher	UPRFL0354
Eupercaria	Tetraodontidae	*Canthigaster rapaensis*	USNM 400531	USNM AG9RO95
Eupercaria	Tetraodontidae	*Canthigaster rostrata*	No voucher	UPRFL0412
Eupercaria	Tetraodontidae	*Canthigaster solandri*	USNM 400518	USNM AG9RM90
Eupercaria	Tetraodontidae	*Canthigaster solandri*	SAIAB 78221	KUIT 7224
Eupercaria	Tetraodontidae	*Canthigaster valentini*	USNM 390990	USNM AG5NP15
Eupercaria	Tetraodontidae	*Chelonodontops patoca*	CSIRO unreg LM921	CSIRO IN02921
Eupercaria	Tetraodontidae	*Feroxodon multistriatus*	CSIRO unreg	CSIRO GT 4433
Eupercaria	Tetraodontidae	*Feroxodon multistriatus*	CSIRO H 8257-01	CSIRO GT 10714
Eupercaria	Tetraodontidae	*Lagocephalus cheesemanii*	CSIRO H 7285-04	CSIRO GT 6570
Eupercaria	Tetraodontidae	*Lagocephalus guentheri*	USNM 437742	USNM AC1VJ91
Eupercaria	Tetraodontidae	*Lagocephalus laevigatus*	No voucher	UPRFL1635
Eupercaria	Tetraodontidae	*Lagocephalus* cf. *suezensis*	CSIRO unreg	CSIRO GT4214
Eupercaria	Tetraodontidae	*Lagocephalus spadiceus*	USNM 403468	USNM AG9RG48
Eupercaria	Tetraodontidae	*Sphoeroides annulatus*	HB-1190	STRI BFT05089
Eupercaria	Tetraodontidae	*Sphoeroides dorsalis*	USNM 433079	USNM AB4OP01
Eupercaria	Tetraodontidae	*Sphoeroides greeleyi*	No voucher	UPRFL1637
Eupercaria	Tetraodontidae	*Sphoeroides lobatus*	No voucher	UPRFL1301
Eupercaria	Tetraodontidae	*Sphoeroides maculatus*	USNM 423825	USNM AE2QZ45
Eupercaria	Tetraodontidae	*Sphoeroides marmoratus*	USNM 405093	USNM AD9NE03
Eupercaria	Tetraodontidae	*Sphoeroides nephelus*	USNM 415007	USNM AC4YB58
Eupercaria	Tetraodontidae	*Sphoeroides pachygaster*	USNM 405072	USNM AD9ND61
Eupercaria	Tetraodontidae	*Sphoeroides spengleri*	No voucher	UPRFL0410
Eupercaria	Tetraodontidae	*Sphoeroides testudineus*	USNM 414276	USNM AC8CC45
Eupercaria	Tetraodontidae	*Takifugu niphobles*	No voucher	ANSP 206060 large

Eupercaria	Tetraodontidae	*Torquigener hicksii*	CSIRO H 6451-01	CSIRO GT 741
Eupercaria	Tetraodontidae	*Torquigener parcuspinus*	CSIRO H 8267-06	CSIRO GT 10748
Eupercaria	Triacanthidae	*Pseudotriacanthus strigilifer*	CSIRO H 7217-12	CSIRO IN02762
Eupercaria	Triacanthidae	*Triacanthus nieuhofi*	CSIRO H 8157-03	CSIRO IN02487
Eupercaria	Triacanthidae	*Tripodichthys blochii*	USNM 424823	USNM AH0SW64
Eupercaria	Triacanthodidae	*Atrophacanthus* sp.	USNM 440414	USNM AB4OL14
Eupercaria	Triacanthodidae	*Halimochirurgus centriscoides*	No voucher	ASIZP 0913987
Eupercaria	Triacanthodidae	*Halimochirurgus centriscoides*	CSIRO H 6574-18	CSIRO GT 1416
Eupercaria	Triacanthodidae	*Halimochirurgus* sp.	CSIRO H 7135-19	CSIRO GT 5806
Eupercaria	Triacanthodidae	*Hollardia hollardia*	VIMS 40109	VIMS 40109
Eupercaria	Triacanthodidae	*Hollardia meadi*	USNM 431710	USNM AG9RL06
Eupercaria	Triacanthodidae	*Parahollardia lineata*	VIMS 40107	VIMS 40107
Eupercaria	Triacanthodidae	*Paratriacanthodes retrospinis*	NMV A 29672-007	CSIRO GT 1472
Eupercaria	Triacanthodidae	*Triacanthodes* sp. 1	CSIRO H 6570-33	CSIRO GT 1862

Table S14. List of prior distributions used for node dating in previous studies that included Tetraodontiformes. Lists the hard minimum ages and 95% soft maximum ages, if provided. Indicates whether or not the superfamily Plectocretacicoidea was included in the divergence time estimations.

Clade	Paper	Hard minimum age	95% Soft maximum age	Includes Plectocretacicoidea?
Tetraodontiformes + Lophiiformes	Hughes et al. 2018 (3)	85 Ma	122 Ma	Yes- *Cretatriacanthus guidottii*
Tetraodontiformes	Near et al. 2013 (5)	---	---	No
Tetraodontiformes	Dornburg et al. 2014 (29)	70.08 Ma	109.845 Ma	Yes- *Plectocretacicus clarae*, *Cretatriacanthus guidottii*
Tetraodontiformes	Betancur-R et al. 2013 (1)	85 Ma	122 Ma	Yes- *Cretatriacanthus guidottii*
Tetraodontiformes + Lophiiformes	Chen et al. 2014 (30)	83 Ma	124 Ma	Yes- *Cretatriacanthus guidottii*
Tetraodontiformes	Santini et al. 2009 (31)	59 Ma	98 Ma	Yes- *Plectocretacicus clarae*
Tetraodontiformes	Near et al. 2012 (32)	---	71.4 Ma	No
Diodontidae + Tetraodontidae	Hughes et al. 2018 (3)	50 Ma	85 Ma	N/A
Tetraodontidae	Hughes et al. 2018 (3)	32 Ma	50 Ma	N/A
Tetraodontidae	Betancur-R et al. 2013 (1)	32 Ma	50 Ma	N/A
Diodontidae + Tetraodontidae	Betancur-R et al. 2013 (1)	50 Ma	85 Ma	N/A
Molidae	Betancur-R et al. 2013 (1)	41 Ma	85 Ma	N/A
Aracanidae + Ostraciidae	Betancur-R et al. 2013 (1)	50 Ma	85 Ma	N/A
Balistidae	Betancur-R et al. 2013 (1)	35 Ma	85 Ma	N/A

SI References

1. R. Betancur-R., *et al.*, The Tree of Life and a New Classification of Bony Fishes. *PLoS Curr* **5** (2013).

2. L. C. Hughes, *et al.*, Exon probe sets and bioinformatics pipelines for all levels of fish phylogenomics. *Molecular Ecology Resources* **21**, 816–833 (2021).

3. L. C. Hughes, *et al.*, Comprehensive phylogeny of ray-finned fishes (Actinopterygii) based on transcriptomic and genomic data. *Proc Natl Acad Sci USA* **115**, 6249–6254 (2018).

4. C. Li, G. Ortí, G. Zhang, G. Lu, A practical approach to phylogenomics: the phylogeny of ray-finned fish (Actinopterygii) as a case study. *BMC Evolutionary Biology* **7**, 44 (2007).

5. T. J. Near, *et al.*, Phylogeny and tempo of diversification in the superradiation of spiny-rayed fishes. *Proceedings of the National Academy of Sciences* **110**, 12738–12743 (2013).

6. V. Ranwez, E. J. P. Douzery, C. Cambon, N. Chantret, F. Delsuc, MACSE v2: Toolkit for the Alignment of Coding Sequences Accounting for Frameshifts and Stop Codons. *Molecular Biology and Evolution* **35**, 2582–2584 (2018).

7. K. Katoh, D. M. Standley, MAFFT Multiple Sequence Alignment Software Version 7: Improvements in Performance and Usability. *Molecular Biology and Evolution* **30**, 772–780 (2013).

8. M. Kearse, *et al.*, Geneious Basic: An integrated and extendable desktop software platform for the organization and analysis of sequence data. *Bioinformatics* **28**, 1647–1649 (2012).

9. M. L. Borowiec, AMAS: a fast tool for alignment manipulation and computing of summary statistics. *PeerJ* **4**, e1660 (2016).

10. L.-T. Nguyen, H. A. Schmidt, A. von Haeseler, B. Q. Minh, IQ-TREE: A Fast and Effective Stochastic Algorithm for Estimating Maximum-Likelihood Phylogenies. *Molecular Biology and Evolution* **32**, 268–274 (2015).

11. D. Arcila, *et al.*, Testing the Utility of Alternative Metrics of Branch Support to Address the Ancient Evolutionary Radiation of Tunas, Stromateoids, and Allies (Teleostei: Pelagiaria). *Systematic Biology* (2021) https:/doi.org/10.1093/sysbio/syab018 (September 30, 2021).

12. S. RATNASINGHAM, P. D. N. HEBERT, bold: The Barcode of Life Data System (http://www.barcodinglife.org). *Mol Ecol Notes* **7**, 355–364 (2007).

13. C. Yang, *et al.*, Efficient COI barcoding using high throughput single-end 400 bp sequencing. *BMC Genomics* **21**, 862 (2020).

14. C. Zhang, M. Rabiee, E. Sayyari, S. Mirarab, ASTRAL-III: polynomial time species tree reconstruction from partially resolved gene trees. *BMC Bioinformatics* **19**, 153 (2018).

15. R. Lanfear, B. Calcott, D. Kainer, C. Mayer, A. Stamatakis, Selecting optimal partitioning schemes for phylogenomic datasets. *BMC Evol Biol* **14**, 82 (2014).

16. B. Q. Minh, M. A. T. Nguyen, A. von Haeseler, Ultrafast Approximation for Phylogenetic Bootstrap. *Molecular Biology and Evolution* **30**, 1188–1195 (2013).

17. D. Arcila, J. C. Tyler, Mass extinction in tetraodontiform fishes linked to the Palaeocene–Eocene thermal maximum. *Proc. R. Soc. B.* **284**, 20171771 (2017).

18. J. P. Huelsenbeck, F. Ronquist, MRBAYES: Bayesian inference of phylogenetic trees. *Bioinformatics* **17**, 754–755 (2001).

19. M. Rincon-Sandoval, *et al.*, Evolutionary determinism and convergence associated with water-column transitions in marine fishes. *Proc Natl Acad Sci USA* **117**, 33396–33403 (2020).

20. A. Santaquiteria, *et al.*, Phylogenomics and Historical Biogeography of Seahorses, Dragonets, Goatfishes, and Allies (Teleostei: Syngnatharia): Assessing Factors Driving Uncertainty in Biogeographic Inferences. *Systematic Biology*, syab028 (2021).

21. M. E. Alfaro, *et al.*, Explosive diversification of marine fishes at the Cretaceous–Palaeogene boundary. *Nat Ecol Evol* **2**, 688–696 (2018).

22. A. J. Drummond, A. Rambaut, BEAST: Bayesian evolutionary analysis by sampling trees. *BMC Evol Biol* **7**, 214 (2007).

23. R. Froese, D. Pauly, FishBase. *www.fishbase.org*.

24. R. Kikinis, S. D. Pieper, K. G. Vosburgh, "3D Slicer: A Platform for Subject-Specific Image Analysis, Visualization, and Clinical Support" in *Intraoperative Imaging and Image-Guided Therapy*, F. A. Jolesz, Ed. (Springer, 2014), pp. 277–289.

25. C. R. Scotese, H. Song, B. J. W. Mills, D. G. van der Meer, Phanerozoic paleotemperatures: The earth's changing climate during the last 540 million years. *Earth-Science Reviews* **215**, 103503 (2021).

26. R Core Team, *R: A language and environment for statistical computing* (2020).

27. J. Clavel, A. Brinkworth, OUenv: Climatic/Environment dependent Ornstein-Uhlenbeck model of trait evolution. GitHub Repository. https://github.com/JClavel/OUenv

28. L. J. Revell, phytools: an R package for phylogenetic comparative biology (and other things). *Methods in Ecology and Evolution* **3**, 217–223 (2012).

29. A. Dornburg, J. P. Townsend, M. Friedman, T. J. Near, Phylogenetic informativeness reconciles ray-finned fish molecular divergence times. *BMC Evol Biol* **14**, 169 (2014).

30. W.-J. Chen, *et al.*, New insights on early evolution of spiny-rayed fishes (Teleostei: Acanthomorpha). *Front. Mar. Sci.* **1** (2014).

31. F. Santini, L. J. Harmon, G. Carnevale, M. E. Alfaro, Did genome duplication drive the origin of teleosts? A comparative study of diversification in ray-finned fishes. *BMC Evol Biol* **9**, 194 (2009).

32. T. J. Near, *et al.*, Resolution of ray-finned fish phylogeny and timing of diversification. *Proceedings of the National Academy of Sciences* **109**, 13698–13703 (2012).

33. B. S. Cramer, K. G. Miller, P. J. Barrett, J. D. Wright, Late Cretaceous–Neogene trends in deep ocean temperature and continental ice volume: Reconciling records of benthic foraminiferal geochemistry (δ^{18} O and Mg/Ca) with sea level history. *J. Geophys. Res.* **116**, C12023 (2011).